



# Systematic study on heavy-particle radioactivity of superheavy nuclei $^{297-300}119$

Megha Chandran<sup>1</sup> · V. K. Anjali<sup>1</sup> · K. P. Santhosh<sup>1,2</sup>

Received: 25 May 2024 / Revised: 3 July 2024 / Accepted: 21 July 2024 / Published online: 12 October 2024

© The Author(s), under exclusive licence to China Science Publishing & Media Ltd. (Science Press), Shanghai Institute of Applied Physics, the Chinese Academy of Sciences, Chinese Nuclear Society 2024

## Abstract

In the current study, we examined every possible cluster–daughter combination in the heavy-particle decay of isotopes  $^{297-300}119$  and computed the decay half-lives using the modified generalized liquid drop model (MGLDM) with the preformation factor depending on the disintegration energy. The predicted half-life of every heavy cluster ( $Z_C \geq 32$ ) was within the experimentally observable limits. These results aligned with the predictions of Poenaru et al. [Phys. Rev. Lett. 107, 062503 (2011)] that superheavy nuclei (SHN) with  $Z > 110$  will release heavy particles with a penetrability comparable to or greater than the  $\alpha$ -decay. The half-lives predicted using the MGLDM for clusters  $^{89}\text{Rb}$ ,  $^{91}\text{Rb}$ , and  $^{92}\text{Rb}$  from parents  $^{297}119$ ,  $^{299}119$ , and  $^{300}119$ , respectively, agreed with the predictions of Poenaru et al. [Eur. Phys. J. A 54, 14 (2018)]. It was found that the isotopes of heavy clusters Kr, Rb, Sr, Pa, In, and Cd had half-lives comparable to the  $\alpha$  half-life; and isotopes of clusters I, Xe, and Cs had the minimum half-life ( $10^{-14}$  s). These observations revealed the role of the shell closure ( $Z=82$ ,  $N=82$ , and  $N=126$ ) of the cluster and daughter nuclei in heavy-cluster radioactivity. We predicted that isotope  $^{297,299}119$  decayed by  $4\alpha$  decay chains and isotope  $^{300}119$  decayed by  $6\alpha$  decay chains, while  $^{298}119$  decayed by continuous  $\alpha$  decay chains. The predicted half-lives and modes of decay of the nuclei in the decay chains of  $^{297-300}119$  agreed with the experimental data, proving the reliability of our calculations. The present study determined the most favorable heavy-cluster emissions from these nuclei and provided suitable projectile–target combinations for their synthesis.

**Keywords** Cluster radioactivity · Alpha radioactivity · Superheavy nuclei

## 1 Introduction

The concept of superheavy elements (elements with  $Z \geq 104$ ) was first introduced in 1958 [1]. The synthesis, decay, and identification of superheavy nuclei (SHN) have emerged as significant and popular topics in nuclear physics. The existence of stable nuclei with large  $Z$  values as a result of nuclear shell effects was supported by several theoretical investigations conducted in the 1960s [2, 3]. Despite the immense Coulomb repulsion in the superheavy region, SHN can exist owing to shell closure effects. The

shell effect was found to be especially strong for nuclei with  $Z=126$  and  $N=184$ , pointing to the prediction of an area known as the "island of stability" around higher atomic numbers. This discovery compels scientists to explore the possibility of synthesizing superheavy elements near the predicted magic numbers. In recent studies, proton numbers ( $Z$  values) of 114, 120, 124, and 126 and neutron numbers ( $N$  values) of 172 and 184 have been predicted to be magic numbers [4–8]. Hot fusion [9] and cold fusion [10] have been used in experiments to produce superheavy elements up to Og ( $Z=118$ ). Currently, different trials are in progress to create superheavy elements with  $Z=119$  and 120. Hofmann et al. [11] investigated the reaction of  $^{54}\text{Cr}$  projectiles on  $^{248}\text{Cm}$  targets to examine their production and decay parameters and synthesize a new superheavy element with  $Z=120$ . Khuyagbaatar et al. [12] also performed experiments to synthesize isotopes with  $Z=119$  and 120 using the reactions  $^{50}\text{Ti} + ^{249}\text{Bk}$  and  $^{50}\text{Ti} + ^{249}\text{Cf}$  at the Gesellschaft für Schwerionenforschung

✉ K. P. Santhosh  
drkpsanthosh625@gmail.com

<sup>1</sup> Department of Physics, University of Calicut, Thenhipalam, Kerala 673635, India

<sup>2</sup> School of Pure and Applied Physics, Kannur University, Swami Anandatheertha Campus, Payyanur, Kerala 670327, India

(GSI). Strong theoretical foundations are required to create new elements that can assist experimentalists in conducting research.

Shell closures can be understood by studying the half-lives of various radioactive modes, such as  $\alpha$ -radioactivity and cluster decay. The decay chains of SHN have been determined using these half-lives, as well as the fission half-lives, because they serve as experimental evidence for the production of these elements in fusion reactions. Checking the mode of disintegration of newly produced SHN is a valid way to understand their decay, which typically involves an  $\alpha$ -decay chain accompanied by spontaneous fission (SF). Numerous theoretical investigations have been conducted to determine the probable decay mechanisms of SHN. The two types of decay experimentally observed in SHN so far are  $\alpha$ -decay and SF. Cluster radioactivity (CR) in the trans-lead region has been studied both theoretically and experimentally [13–16]. In 2001, Royer et al. [17] studied light particle emission using the generalized liquid drop model (GLDM) and quasi-molecular shapes and introduced an analytical formula for light nuclear decay. Royer et al. [18] investigated the alpha decay, cluster radioactivity, and heavy-particle emission half-lives of known and still unknown SHN using the original GLDM and analytical formulas, and found that  $^{76-80}\text{Zn}$ ,  $^{78}\text{Ga}$ ,  $^{72,74-76}\text{Cu}$ ,  $^{69,71}\text{Ni}$ , and  $^{47}\text{K}$  nuclei are the best candidates for emission from SHN, with the daughter nuclei being doubly closed  $^{208}\text{Pb}$  or neighboring nuclei. The modified generalized liquid drop model (MGLDM), which developed by introducing the proximity 77 potential of Blocki et al. [19] to the GLDM of Royer and Remaud [20, 21], was used to investigate the emission of even–even light clusters such as Be, C, O, Ne, Mg, and Si from SHN with a  $Z$  value of 120 [22]. The concept of heavy-particle radioactivity (HPR), which permits the release of particles with  $Z_C > 28$  from SHN with  $Z > 110$ , was proposed by Poenaru et al. [23] in 2011. This concept predicted that HPR is more probable than  $\alpha$  decay in SHN. Zhang and Wang [24] employed the universal decay law (UDL) formula to predict the supremacy of cluster decay over  $\alpha$  decay. The Coulomb and proximity potential model for deformed nuclei (CPPMDN) [25], which is a productive approach, was able to forecast HPR with a half-life similar to or even dominant over  $\alpha$  decay for isotopes with  $Z \geq 118$ . The investigation on the HPR from superheavy elements with  $Z = 118$  and  $Z = 120$  employing the MGLDM with a  $Q$ -value-dependent preformation factor [26, 27] was effective in obtaining half-lives comparable to  $\alpha$  half-lives. In 2021, Qian et al. [28] studied the surface alpha clustering in heavy nuclei by considering the preformation factor, which behaves with a Geiger-Nuttal-like pattern (i.e.,  $P_C$  has an exponent law with  $Q^{-1/2}$ ). Later, Wan et al. [29] considered the  $\alpha$ -decay energies and half-lives of SHN within the cluster model, along with a slightly modified Woods–Saxon potential.

Using the MGLDM, we studied heavy-cluster emissions ( $Z_C > 28$ ) from  $Z = 118$  [26] and  $Z = 120$  [27], leading to doubly magic  $^{208}\text{Pb}$  or its neighbor (the obtained half-lives were comparable to the  $\alpha$  half-lives) and doubly magic  $^{132}\text{Sn}$  or its neighbor (with minimum half-lives). In a previous study [22] we considered the cluster decay of various isotopes of  $Z = 120$  emitting light clusters ( $Z_C < 14$ ) ranging from  $^8\text{Be}$  to  $^{34}\text{Si}$  using the MGLDM. It should be noted that in this study, the residual nuclei formed were neither doubly magic  $^{208}\text{Pb}$ ,  $^{132}\text{Sn}$ , nor neighboring nuclei.

The goal of the current study was to examine every possible combination of cluster daughters in heavy clusters for isotopes  $^{297-300}119$  and compute all the heavy-cluster decay half-lives using the MGLDM with the  $Q$ -value-dependent preformation factor. Section 2 outlines the theoretical framework of the study. The findings of this study and their significance are presented in Sect. 3. Finally, Sect. 4 concludes the study.

## 2 MGLDM

In the MGLDM, the total energy of the decaying nucleus is found as follows:

$$E = E_V + E_S + E_C + E_R + E_P. \quad (1)$$

For the post-scission zone, the volume, surface, and Coulomb energies were provided by Royer et al. [20] as follows:

$$E_V = -15.494[(1 - 1.8I_1^2)A_1 + (1 - 1.8I_2^2)A_2], \quad (2)$$

$$E_S = 17.9439 \left[ (1 - 2.6I_1^2)A_1^{2/3} + (1 - 2.6I_2^2)A_2^{2/3} \right], \quad (3)$$

$$E_C = \frac{0.6e^2Z_1^2}{R_1} + \frac{0.6e^2Z_2^2}{R_2} + \frac{e^2Z_1Z_2}{r}, \quad (4)$$

where  $A_i$  represents the mass,  $Z_i$  represents the charge,  $R_i$  represents the radius,  $I_i$  represents the relative neutron excess of the two nuclei, and  $r$  represents the separation between the mass centers. The nuclear proximity energy [19] is found as follows:

$$E_P(z) = 4\pi\gamma b \left[ \frac{C_1C_2}{(C_1 + C_2)} \right] \Phi\left(\frac{z}{b}\right), \quad (5)$$

where  $\gamma$  is the nuclear surface tension coefficient, and  $\Phi$  is the universal proximity potential [30].

Tunneling probability  $P$  [20] is found as follows:

$$P = \exp \left\{ -\frac{2}{\hbar} \int_{R_{\text{in}}}^{R_{\text{out}}} \sqrt{2B(r)[E(r) - E(\text{sphere})]} dr \right\}, \quad (6)$$

where  $R_{\text{in}} = R_1 + R_2$ ,  $R_{\text{out}} = e^2Z_1Z_2/Q$ , and mass inertia  $B(r) = \mu$ , the reduced mass.

The partial half-life can be computed as follows:

$$T_{1/2} = \left( \frac{\ln 2}{\lambda} \right) = \left( \frac{\ln 2}{\nu P_C P} \right). \quad (7)$$

Here  $P_C$ , the preformation probability [31], is found as follows:

$$P_C = 10^{aQ+bQ^2+c} \quad (8)$$

with  $a = -0.25736$ ,  $b = 6.37291 \times 10^{-4}$ , and  $c = 3.35106$ . For alpha decay, the preformation factors [32] ( $P_C = 0.94$  for even–even nuclei,  $P_C = 0.85$  for odd– $A$  nuclei, and  $P_C = 0.67$  for doubly odd nuclei) were obtained using the MGLDM values and experimental data of 318 nuclei in the range of  $Z = 74$  to 93. Assault frequency  $\nu = \frac{\omega}{2\pi} = \frac{2E_v}{h}$ , where  $E_v$  is the zero-point vibration energy, which is given as follows [16]:

$$E_v = Q \left\{ 0.056 + 0.039 \exp \left[ \frac{(4 - A_2)}{2.5} \right] \right\}, \text{ for } A_2 \geq 4. \quad (9)$$

### 3 Results and discussion

The possible heavy-particle radiations from SHN with  $Z = 119$  and  $297 \leq A \leq 300$  were investigated using the MGLDM with a  $Q$ -value-dependent preformation factor. In our previous work [31], we studied cluster radioactivity from various heavy nuclei using the MGLDM with  $Q$ -value-dependent preformations. In this study, we estimated the accuracy of our predicted half-lives and found that they matched the  $T_{1/2}^{\text{Exp}}$  values with a standard deviation of 0.755. We have also studied the  $\alpha$  decay of various SHN [33] using the MGLDM and the predicted half-lives were found to have the values, with a least standard deviation of 0.34.

The preformation factor is not a measurable quantity but a hypothetical and model-dependent one. The  $Q$  value differs for various clusters radiating from the same mother nucleus and for the same cluster emitted from different mother nuclei. This has been confirmed experimentally [34, 35]. The relevance of  $Q$  values, which characterize the decay process, led to the study [36] of the variation of the  $Q$  value with the cluster preformation probability extracted from experimental data [34, 35], with their obtained relation given in Eq. (8). The constants in this equation were obtained by the least-squares fitting of the experimental cluster decay data [34, 35]. In the expression for the tunneling probability, Eq. (6), the inner turning point,  $R_{\text{in}}$ , is considered the contact point, which is valid for alpha emission. In the case of heavy-particle emission, we considered the contribution of the overlapping region (the internal part of the barrier)

when developing the  $Q$ -dependent preformation factor, as shown in Eq. (8).

All of the cluster–daughter decay combinations for  $^{297}119$ ,  $^{298}119$ ,  $^{299}119$ , and  $^{300}119$ , which had positive  $Q$  values, were evaluated. The disintegration energy is given by the following:

$$Q = \Delta M_p - (\Delta M_d + \Delta M_c), \quad (10)$$

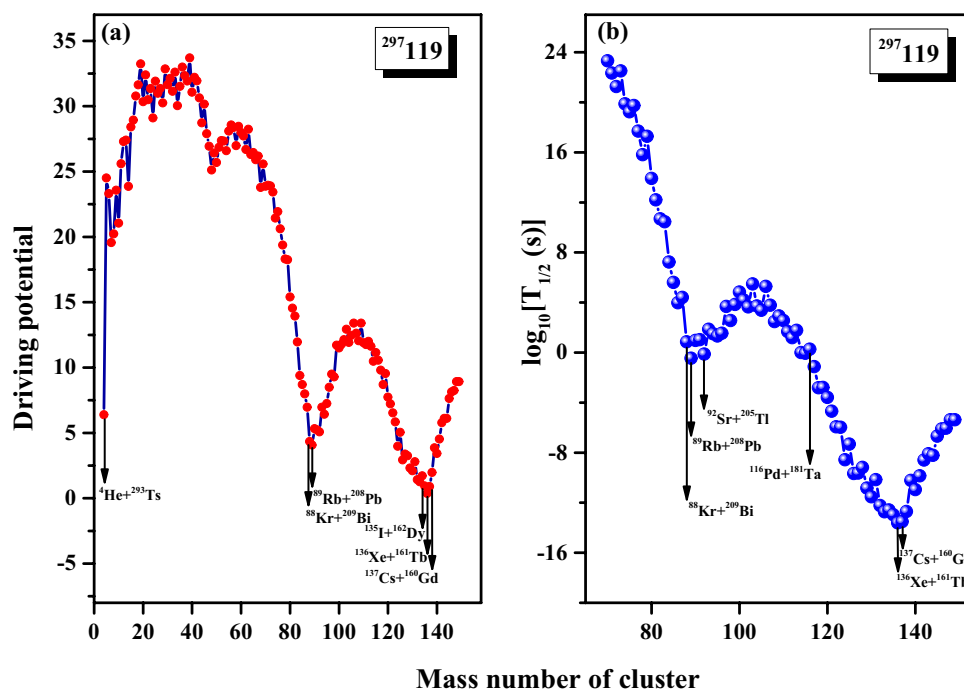
where  $\Delta M_p$  is the difference in the mass excess of the parent, and  $\Delta M_d$  and  $\Delta M_c$  are the differences in the mass excesses of the two decay products. These data were taken from the AME2020 mass tables of Wang et al. [37], and on a few occasions, the KTUY05 table [38] was used for some nuclei whose experimental values were unavailable. A comprehensive study of the  $\alpha$ -decay energies,  $Q$  values, and half-lives of 121 SHN with  $Z > 100$  was performed using twenty mass tables by Wang et al. [39]. The results showed that the KUTY05 mass model was the best at reproducing the experimental  $Q$  values of the SHN, and the standard deviation in the estimation of the  $Q$  value was 0.352.

Our current research had the goal of understanding the characteristics of SHN, specifically those for  $Z = 119$  with  $297 \leq A \leq 300$ . We examined all the potential cluster–daughter combinations using a cold reaction valley plot, which connects the driving potential with the mass number of the cluster. This plot was used to analyze the valleys or low-energy regions in the driving potential. Driving potential refers to the overall energy difference between the interaction potential ( $V$ ) and the disintegration energy ( $Q$  value) associated with the reaction process. The driving potential ( $V - Q$ ) is computed for the parent nucleus by taking into account the variations in mass and charge asymmetries,  $\eta_A = \frac{A_1 - A_2}{A_1 + A_2}$  and  $\eta_Z = \frac{Z_1 - Z_2}{Z_1 + Z_2}$ , for the touching configuration.

In the touching configuration, the distance between fragments ( $r$ ) is equal to the sum of the Sussman central radii ( $C_1$  and  $C_2$ ). For a certain value of mass asymmetry ( $\eta_A$ ) and separation among the fragments ( $r$ ), the charges of the fragments are determined by minimizing the driving potential. In other words, for a given set of masses ( $A_1, A_2$ ) in the mass–asymmetric coordinate system, the specific set ( $Z_1, Z_2$ ) that yields the lowest driving potential is found. The minimum driving potential corresponds to the most probable decay for a specific pair ( $A_1, A_2$ ).

Figures 1(a), 2(a), 3(a), and 4(a) plot the driving potentials with the mass numbers of clusters for  $^{297}119$ ,  $^{298}119$ ,  $^{299}119$ , and  $^{300}119$  respectively. Decay combination [ $^{136}\text{Xe}$  ( $N = 82$ ) +  $^{161}\text{Tb}$ ] exhibits the lowest driving potential among all the possibilities for isotope  $^{297}119$ , suggesting that it is the most likely decay to occur. Likewise, other combinations such as [ $^{135}\text{I}$  ( $N = 82$ ) +  $^{162}\text{Dy}$ ] and [ $^{137}\text{Cs}$  ( $N = 82$ ) +  $^{160}\text{Gd}$ ], where the cluster nuclei possess a magic number of neutrons, demonstrate relatively lower driving potentials. For

**Fig. 1** **a** Plot of driving potential vs. mass number of clusters for  $^{297}119$  for touching configuration  $r = C_1 + C_2$ . **b** Variation of logarithm of half-life with mass number of clusters for probable heavy-cluster decay from  $^{297}119$



$^{298}119$ , [ $^{135}\text{I}$  ( $N=82$ ) +  $^{163}\text{Dy}$ ] is the combination with the minimum driving potential. The decay combination [ $^{134}\text{I}$  ( $N=81$ ) +  $^{164}\text{Dy}$ ] also has a comparatively low driving potential. The decay combination [ $^{134}\text{Te}$  ( $N=82$ ) +  $^{165}\text{Ho}$ ] shows the minimum driving potential compared to all the other possibilities for isotope  $^{299}119$ . For  $^{300}119$ , the decay combination involving [ $^{133}\text{Te}$  ( $N=81$ ) +  $^{167}\text{Ho}$ ] shows the least driving potential. Based on all these cases, it can be concluded that the decay combination with the minimum driving potential, which is the most likely degradation, is formed in a manner where the cluster nuclei possess a magic number of neutrons.

The half-lives were calculated using the MGLDM for all the possible heavy-particle emissions linked to each  $Z=119$  isotope after the fragment combination was determined. The obtained  $T_{1/2}$  values of the possible heavy clusters for  $^{297-300}119$  are listed in Tables 1 and 2. Columns 1 and 5 give the probable clusters. Columns 2 and 6 give the daughters. Columns 3 and 7 give the  $Q$  values, and columns 4 and 8 give the heavy-particle decay half-lives in seconds. For the half-life of any heavy cluster ( $Z_C \geq 32$ ) predicted in Tables 1 and 2 that is within experimentally observable limits. Our findings were consistent with the predictions of Poenaru et al. [23] that SHN with  $Z > 110$  release heavy clusters with  $Z_C > 28$ . In some circumstances, the likelihood of heavy-particle decay is greater than the probability of alpha decay according to the heavy-particle radioactivity concept of Poenaru et al. [23]. Given the measurable half-lives ( $\leq 10^{12}$  s) obtained, more advanced nuclear beam sources such as China's High-Intensity Heavy-Ion Accelerator Facility (HIAF) are required to assess the potential

for heavy-cluster radioactivity. Poenaru et al. [40] studied cluster and  $\alpha$  emissions for SHN with  $Z=119$  and 120. Two models, the analytical super asymmetric fission model (ASAFM) and universal formula (UNIV) were used by the authors to calculate the half-lives of cluster radioactivity.

Table 3 compares the half-lives obtained using the present formalism for clusters  $^{89}\text{Rb}$ ,  $^{91}\text{Rb}$ , and  $^{92}\text{Rb}$  from parents  $^{297}119$ ,  $^{299}119$ , and  $^{300}119$ , respectively, along with the values reported by Poenaru et al. [40]. Our predictions match the values reported by Poenaru et al., emphasizing the reliability of our calculations.

The emission of clusters of C, O, F, Ne, Mg, and Si from heavy nuclei ranging from  $^{221}\text{Fr}$  to  $^{242}\text{Cm}$  was experimentally observed [34, 35], in which the daughters consistently exhibited a doubly magic configuration such as  $^{208}\text{Pb}$  or a neighboring one. It should be noted that several researchers have used different models to study the emission of light clusters of C, O, F, Ne, Mg, Si, etc. from SHN. In these decays, the daughter was not the doubly magic  $^{208}\text{Pb}$  or a neighboring one, but none of them succeeded in predicting a half-life equivalent to that of the  $\alpha$ -decay. Only a few models have successfully been used to study heavy particle radioactivity ( $Z_C > 28$ ) from SHN with  $Z > 110$ , in which the half-lives obtained were comparable to the alpha half-lives, and the decays led to  $^{208}\text{Pb}$  or neighboring nuclei. The first model to predict heavy-cluster decay half-lives comparable to alpha half-lives was the ASAFM of Poenaru et al. [23]; the other models were the CPPM [25] and MGLDM [26]. Recently, Ghodsi et al. [41] studied heavy-cluster decay from SHN using a double-folding formalism. Their results were compared with those of other models, including our results

**Table 1** Predicted half-lives of probable clusters from SHN<sup>297, 298</sup>119

Parent nuclei— <sup>297</sup> 119				Parent nuclei— <sup>298</sup> 119			
Emitted cluster	Daughter nuclei	<i>Q</i> value (MeV)	<i>T</i> <sub>1/2</sub> (s)	Emitted cluster	Daughter nuclei	<i>Q</i> value (MeV)	<i>T</i> <sub>1/2</sub> (s)
<sup>4</sup> He	<sup>293</sup> Ts	10.4651	2.76 × 10 <sup>0</sup>	<sup>4</sup> He	<sup>294</sup> Ts	10.33508	7.89 × 10 <sup>0</sup>
<sup>81</sup> As	<sup>216</sup> Rn	279.6003	1.57 × 10 <sup>12</sup>	<sup>82</sup> As	<sup>216</sup> Rn	279.0120	2.24 × 10 <sup>12</sup>
<sup>82</sup> Se	<sup>215</sup> At	286.1709	4.76 × 10 <sup>10</sup>	<sup>83</sup> As	<sup>215</sup> Rn	279.9983	2.36 × 10 <sup>11</sup>
<sup>83</sup> As	<sup>214</sup> Rn	281.3093	2.84 × 10 <sup>10</sup>	<sup>84</sup> Se	<sup>214</sup> At	288.4867	1.65 × 10 <sup>8</sup>
<sup>84</sup> Se	<sup>213</sup> At	289.8477	1.73 × 10 <sup>7</sup>	<sup>85</sup> Br	<sup>213</sup> Po	294.3890	1.11 × 10 <sup>7</sup>
<sup>85</sup> Br	<sup>212</sup> Po	296.2644	4.07 × 10 <sup>5</sup>	<sup>86</sup> Br	<sup>212</sup> Po	295.1614	1.55 × 10 <sup>6</sup>
<sup>86</sup> Kr	<sup>211</sup> Bi	302.4447	9.42 × 10 <sup>3</sup>	<sup>87</sup> Kr	<sup>211</sup> Bi	301.7285	1.62 × 10 <sup>4</sup>
<sup>87</sup> Br	<sup>210</sup> Po	297.1651	2.54 × 10 <sup>4</sup>	<sup>88</sup> Kr	<sup>210</sup> Bi	303.6432	1.68 × 10 <sup>2</sup>
<sup>88</sup> Kr	<sup>209</sup> Bi	305.2699	7.13 × 10 <sup>0</sup>	<sup>89</sup> Kr	<sup>209</sup> Bi	303.9544	4.96 × 10 <sup>1</sup>
<sup>89</sup> Rb	<sup>208</sup> Pb	310.7805	3.49 × 10 <sup>-1</sup>	<sup>90</sup> Rb	<sup>208</sup> Pb	310.2745	3.64 × 10 <sup>-1</sup>
<sup>90</sup> Rb	<sup>207</sup> Pb	309.1380	9.33 × 10 <sup>0</sup>	<sup>91</sup> Rb	<sup>207</sup> Pb	309.3570	1.88 × 10 <sup>0</sup>
<sup>91</sup> Rb	<sup>206</sup> Pb	308.8505	1.08 × 10 <sup>1</sup>	<sup>92</sup> Sr	<sup>206</sup> Tl	314.2803	2.22 × 10 <sup>-1</sup>
<sup>92</sup> Rb	<sup>205</sup> Tl	314.0078	7.55 × 10 <sup>-1</sup>	<sup>93</sup> Sr	<sup>205</sup> Tl	313.0668	2.26 × 10 <sup>0</sup>
<sup>93</sup> Sr	<sup>204</sup> Tl	311.7521	7.31 × 10 <sup>1</sup>	<sup>94</sup> Sr	<sup>204</sup> Tl	312.3518	7.13 × 10 <sup>0</sup>
<sup>94</sup> Sr	<sup>203</sup> Tl	311.9270	3.20 × 10 <sup>1</sup>	<sup>95</sup> Y	<sup>203</sup> Hg	315.6372	2.06 × 10 <sup>1</sup>
<sup>95</sup> Y	<sup>202</sup> Hg	315.8733	2.10 × 10 <sup>1</sup>	<sup>96</sup> Y	<sup>202</sup> Hg	314.8353	7.72 × 10 <sup>1</sup>
<sup>96</sup> Zr	<sup>201</sup> Au	319.1599	3.53 × 10 <sup>1</sup>	<sup>97</sup> Zr	<sup>201</sup> Au	318.4977	5.77 × 10 <sup>1</sup>
<sup>97</sup> Y	<sup>200</sup> Hg	312.9383	4.88 × 10 <sup>3</sup>	<sup>98</sup> Zr	<sup>200</sup> Au	317.6820	2.23 × 10 <sup>2</sup>
<sup>98</sup> Zr	<sup>199</sup> Au	317.6958	3.63 × 10 <sup>2</sup>	<sup>99</sup> Zr	<sup>199</sup> Au	315.8708	6.86 × 10 <sup>3</sup>
<sup>99</sup> Nb	<sup>198</sup> Pt	319.5590	7.01 × 10 <sup>3</sup>	<sup>100</sup> Zr	<sup>198</sup> Au	315.1138	2.35 × 10 <sup>4</sup>
<sup>100</sup> Zr	<sup>197</sup> Au	314.8328	6.87 × 10 <sup>4</sup>	<sup>101</sup> Nb	<sup>197</sup> Pt	318.4708	2.08 × 10 <sup>4</sup>
<sup>101</sup> Nb	<sup>196</sup> Pt	318.8555	1.56 × 10 <sup>4</sup>	<sup>102</sup> Nb	<sup>196</sup> Pt	318.1028	3.25 × 10 <sup>4</sup>
<sup>102</sup> Mo	<sup>195</sup> Ir	322.5733	4.39 × 10 <sup>3</sup>	<sup>103</sup> Mo	<sup>195</sup> Ir	321.8063	9.42 × 10 <sup>3</sup>
<sup>103</sup> Nb	<sup>194</sup> Pt	317.1091	3.02 × 10 <sup>5</sup>	<sup>104</sup> Mo	<sup>194</sup> Ir	322.0358	4.39 × 10 <sup>3</sup>
<sup>104</sup> Mo	<sup>193</sup> Ir	322.2003	5.22 × 10 <sup>3</sup>	<sup>105</sup> Mo	<sup>193</sup> Ir	321.0273	2.62 × 10 <sup>4</sup>
<sup>105</sup> Tc	<sup>192</sup> Os	325.4923	2.38 × 10 <sup>3</sup>	<sup>106</sup> Tc	<sup>192</sup> Os	324.8183	4.29 × 10 <sup>3</sup>
<sup>106</sup> Mo	<sup>191</sup> Ir	320.1568	1.96 × 10 <sup>5</sup>	<sup>107</sup> Tc	<sup>191</sup> Os	324.3052	9.40 × 10 <sup>3</sup>
<sup>107</sup> Tc	<sup>190</sup> Os	324.7778	5.97 × 10 <sup>3</sup>	<sup>108</sup> Ru	<sup>190</sup> Re	328.4040	7.16 × 10 <sup>2</sup>
<sup>108</sup> Ru	<sup>189</sup> Re	328.9600	2.96 × 10 <sup>2</sup>	<sup>109</sup> Ru	<sup>189</sup> Re	327.8770	1.26 × 10 <sup>3</sup>
<sup>109</sup> Rh	<sup>188</sup> W	330.9870	8.38 × 10 <sup>2</sup>	<sup>110</sup> Ru	<sup>188</sup> Re	328.2499	4.52 × 10 <sup>2</sup>
<sup>110</sup> Ru	<sup>187</sup> Re	328.6095	3.65 × 10 <sup>2</sup>	<sup>111</sup> Rh	<sup>187</sup> W	331.3680	1.37 × 10 <sup>2</sup>
<sup>111</sup> Rh	<sup>186</sup> W	332.1326	4.77 × 10 <sup>1</sup>	<sup>112</sup> Rh	<sup>186</sup> W	331.3986	1.00 × 10 <sup>2</sup>
<sup>112</sup> Pd	<sup>185</sup> Ta	335.0350	1.54 × 10 <sup>1</sup>	<sup>113</sup> Rh	<sup>185</sup> W	331.3149	9.40 × 10 <sup>1</sup>
<sup>113</sup> Rh	<sup>184</sup> W	331.7925	5.98 × 10 <sup>1</sup>	<sup>114</sup> Pd	<sup>184</sup> Ta	335.4890	2.08 × 10 <sup>0</sup>
<sup>114</sup> Pd	<sup>183</sup> Ta	336.1035	9.91 × 10 <sup>-1</sup>	<sup>115</sup> Pd	<sup>183</sup> Ta	334.8795	6.00 × 10 <sup>0</sup>
<sup>115</sup> Ag	<sup>182</sup> Hf	338.3530	8.78 × 10 <sup>-1</sup>	<sup>116</sup> Pd	<sup>182</sup> Ta	335.4217	1.50 × 10 <sup>0</sup>
<sup>116</sup> Pd	<sup>181</sup> Ta	335.5901	1.86 × 10 <sup>0</sup>	<sup>117</sup> Ag	<sup>181</sup> Hf	338.7450	1.33 × 10 <sup>-1</sup>
<sup>117</sup> Ag	<sup>180</sup> Hf	339.2815	7.53 × 10 <sup>-2</sup>	<sup>118</sup> Cd	<sup>180</sup> Lu	342.5420	2.74 × 10 <sup>-3</sup>
<sup>118</sup> Cd	<sup>179</sup> Lu	343.0810	1.54 × 10 <sup>-3</sup>	<sup>119</sup> Cd	<sup>179</sup> Lu	342.1990	4.66 × 10 <sup>-3</sup>
<sup>119</sup> In	<sup>178</sup> Yb	344.6960	1.63 × 10 <sup>-3</sup>	<sup>120</sup> Cd	<sup>178</sup> Lu	343.4549	2.17 × 10 <sup>-4</sup>
<sup>120</sup> Cd	<sup>177</sup> Lu	343.6609	2.61 × 10 <sup>-4</sup>	<sup>121</sup> In	<sup>177</sup> Yb	345.9814	4.85 × 10 <sup>-5</sup>
<sup>121</sup> In	<sup>176</sup> Yb	346.6463	2.03 × 10 <sup>-5</sup>	<sup>122</sup> In	<sup>176</sup> Yb	346.2213	2.20 × 10 <sup>-5</sup>
<sup>122</sup> Sn	<sup>175</sup> Tm	349.5700	1.16 × 10 <sup>-6</sup>	<sup>123</sup> In	<sup>175</sup> Yb	347.2846	1.38 × 10 <sup>-6</sup>
<sup>123</sup> In	<sup>174</sup> Yb	347.6935	1.06 × 10 <sup>-6</sup>	<sup>124</sup> Sn	<sup>174</sup> Tm	351.2515	5.07 × 10 <sup>-9</sup>
<sup>124</sup> Sn	<sup>173</sup> Tm	351.8075	2.67 × 10 <sup>-9</sup>	<sup>125</sup> Sn	<sup>173</sup> Tm	351.3097	3.35 × 10 <sup>-9</sup>
<sup>125</sup> Sn	<sup>172</sup> Tm	350.5877	4.80 × 10 <sup>-8</sup>	<sup>126</sup> Sn	<sup>172</sup> Tm	352.5490	8.41 × 10 <sup>-11</sup>
<sup>126</sup> Sn	<sup>171</sup> Tm	352.5453	2.13 × 10 <sup>-10</sup>	<sup>127</sup> Sn	<sup>171</sup> Tm	351.8403	4.74 × 10 <sup>-10</sup>
<sup>127</sup> Sb	<sup>170</sup> Er	354.1255	2.31 × 10 <sup>-10</sup>	<sup>128</sup> Sn	<sup>170</sup> Tm	352.3163	9.46 × 10 <sup>-11</sup>

**Table 1** (continued)

Parent nuclei— <sup>297</sup> 119				Parent nuclei— <sup>298</sup> 119			
Emitted cluster	Daughter nuclei	<i>Q</i> value (MeV)	<i>T</i> <sub>1/2</sub> (s)	Emitted cluster	Daughter nuclei	<i>Q</i> value (MeV)	<i>T</i> <sub>1/2</sub> (s)
<sup>128</sup> Sn	<sup>169</sup> Tm	351.9557	6.59 × 10 <sup>-10</sup>	<sup>129</sup> Sb	<sup>169</sup> Er	354.7102	1.07 × 10 <sup>-11</sup>
<sup>129</sup> Sb	<sup>168</sup> Er	354.9382	1.46 × 10 <sup>-11</sup>	<sup>130</sup> Te	<sup>168</sup> Ho	356.5730	3.34 × 10 <sup>-12</sup>
<sup>130</sup> Te	<sup>167</sup> Ho	356.9520	2.98 × 10 <sup>-12</sup>	<sup>131</sup> Te	<sup>167</sup> Ho	356.6500	2.14 × 10 <sup>-12</sup>
<sup>131</sup> Sb	<sup>166</sup> Er	354.2255	6.99 × 10 <sup>-11</sup>	<sup>132</sup> Te	<sup>166</sup> Ho	357.4183	2.79 × 10 <sup>-13</sup>
<sup>132</sup> Te	<sup>165</sup> Ho	357.4060	5.88 × 10 <sup>-13</sup>	<sup>133</sup> Te	<sup>165</sup> Ho	356.9951	5.85 × 10 <sup>-13</sup>
<sup>133</sup> I	<sup>164</sup> Dy	359.1446	1.85 × 10 <sup>-13</sup>	<sup>134</sup> I	<sup>164</sup> Dy	359.1706	8.65 × 10 <sup>-14</sup>
<sup>134</sup> Xe	<sup>163</sup> Tb	360.0418	2.63 × 10 <sup>-13</sup>	<sup>135</sup> I	<sup>163</sup> Dy	359.3201	6.44 × 10 <sup>-14</sup>
<sup>135</sup> I	<sup>162</sup> Dy	359.2804	1.10 × 10 <sup>-13</sup>	<sup>136</sup> Cs	<sup>162</sup> Gd	359.7800	1.90 × 10 <sup>-12</sup>
<sup>136</sup> Xe	<sup>161</sup> Tb	361.2110	2.47 × 10 <sup>-14</sup>	<sup>137</sup> Cs	<sup>161</sup> Gd	361.2119	4.91 × 10 <sup>-14</sup>
<sup>137</sup> Cs	<sup>160</sup> Gd	361.8079	3.05 × 10 <sup>-14</sup>	<sup>138</sup> Cs	<sup>160</sup> Gd	359.9891	7.99 × 10 <sup>-13</sup>
<sup>138</sup> Ba	<sup>159</sup> Eu	361.6248	1.97 × 10 <sup>-13</sup>	<sup>139</sup> Ba	<sup>159</sup> Eu	360.1169	3.98 × 10 <sup>-12</sup>
<sup>139</sup> Cs	<sup>158</sup> Gd	358.7110	6.03 × 10 <sup>-11</sup>	<sup>140</sup> Ba	<sup>158</sup> Eu	359.6985	1.12 × 10 <sup>-11</sup>
<sup>140</sup> Ba	<sup>157</sup> Eu	360.0470	1.12 × 10 <sup>-11</sup>	<sup>141</sup> Ba	<sup>157</sup> Eu	358.3510	3.63 × 10 <sup>-10</sup>
<sup>141</sup> La	<sup>156</sup> Sm	359.6110	1.40 × 10 <sup>-10</sup>	<sup>142</sup> La	<sup>156</sup> Sm	358.5450	8.32 × 10 <sup>-10</sup>
<sup>142</sup> Ce	<sup>155</sup> Pm	358.7929	2.58 × 10 <sup>-9</sup>	<sup>143</sup> La	<sup>155</sup> Sm	357.5222	1.00 × 10 <sup>-8</sup>
<sup>143</sup> La	<sup>154</sup> Sm	357.9466	8.05 × 10 <sup>-9</sup>	<sup>144</sup> Ce	<sup>154</sup> Pm	357.8589	1.01 × 10 <sup>-8</sup>
<sup>144</sup> Ce	<sup>153</sup> Pm	358.3999	6.11 × 10 <sup>-9</sup>	<sup>145</sup> Ce	<sup>153</sup> Pm	356.8780	1.03 × 10 <sup>-7</sup>
<sup>145</sup> Pr	<sup>152</sup> Nd	357.0960	2.05 × 10 <sup>-7</sup>	<sup>146</sup> Ce	<sup>152</sup> Pm	356.0400	7.21 × 10 <sup>-7</sup>
<sup>146</sup> Ce	<sup>151</sup> Pm	356.3320	7.88 × 10 <sup>-7</sup>	<sup>147</sup> Pr	<sup>151</sup> Nd	355.5472	3.32 × 10 <sup>-6</sup>
<sup>147</sup> Pr	<sup>150</sup> Nd	356.4440	8.99 × 10 <sup>-7</sup>	<sup>148</sup> Pr	<sup>150</sup> Nd	355.3750	4.86 × 10 <sup>-6</sup>
<sup>149</sup> Pr	<sup>148</sup> Nd	355.7671	4.22 × 10 <sup>-6</sup>	<sup>149</sup> Pr	<sup>149</sup> Nd	354.5745	2.97 × 10 <sup>-5</sup>

using the CPPM [25], and agreed with our findings. In the present work, our group considered all of the probable heavy clusters in the frame of the MGLDM and predicted half-lives comparable to those of the  $\alpha$  half-lives (decays leading to the doubly magic <sup>208</sup>Pb or a neighboring one), along with the minimum half-lives (decays leading to the doubly magic <sup>132</sup>Sn or a neighboring one). It should be emphasized that the predictions of HPR half-lives comparable to the alpha decay half-lives in the superheavy region are model-dependent. In Ref. [25], we studied the HPR ( $Z_C > 28$ ) from the isotopes of SHN using the CPPM with the preformation probability, which depends on the  $Q$  value of the decay. In the current study, we used the MGLDM with a  $Q$ -value-dependent preformation probability to study the HPR from isotopes of  $Z = 119$ . In Ref. [31], we analyzed the emission of light clusters ( $Z_C < 14$ ) of C, O, F, Ne, Mg, and Si from various heavy nuclei with  $A$  values ranging from 221 to 242 using the MGLDM with a  $Q$ -dependent preformation factor. The former study [25] dealt with the emission of heavy clusters from SHN, whereas the latter one [31] dealt with the study of light clusters from heavy nuclei. We would like to mention that the models used for these studies were different. In the CPPM and MGLDM, the expressions used for the barrier penetrability were different (see Eq. (5) of Ref. [25] and Eq. (14) of Ref. [31], respectively).

The variation in the  $\log_{10}T_{1/2}$  value of the probable heavy cluster versus the mass number of the cluster for the possible HPR from <sup>297</sup>119 is depicted in Fig. 1(b). The half-life decreased with increasing cluster size. In addition, the predicted heavy-cluster decay half-life exhibited peaks and dips. The stability of the mother nucleus was represented by the half-life peak, whereas the durability of the decay fragments was represented by the half-life drop. When decay fragments have closed shells, they are more likely to be stable and undergo radioactive decay. In Fig. 1(b), the small dip in the half-life corresponds to the fragment combinations [<sup>86</sup>Kr ( $N = 50$ ) + <sup>211</sup>Bi], [<sup>89</sup>Rb + <sup>208</sup>Pb ( $N = 126$ )], [<sup>124</sup>Sn ( $Z = 50$ ) + <sup>173</sup>Tm], [<sup>136</sup>Xe ( $N = 82$ ) + <sup>161</sup>Tb], and [<sup>137</sup>Cs ( $N = 82$ ) + <sup>160</sup>Gd]. This indicates that if the daughter or cluster possesses a magic number of neutrons or protons, a dip in the decay half-life can be observed.

The same observation was made for <sup>298</sup>119, <sup>299</sup>119, and <sup>300</sup>119. In Fig. 2(b), the small dip in half-life corresponds to fragment combinations [<sup>90</sup>Rb + <sup>208</sup>Pb ( $N = 126$ )], [<sup>126</sup>Sn ( $Z = 50$ ) + <sup>172</sup>Tm], [<sup>135</sup>I ( $N = 82$ ) + <sup>163</sup>Dy], and [<sup>137</sup>Cs ( $N = 82$ ) + <sup>161</sup>Gd]. As shown in Fig. 3(b), fragment combinations [<sup>92</sup>Sr + <sup>207</sup>Tl ( $N = 126$ )], [<sup>126</sup>Sn ( $Z = 50$ ) + <sup>173</sup>Tm], and [<sup>136</sup>Xe ( $N = 82$ ) + <sup>163</sup>Tb] exhibited the lowest half-lives. The minimum  $T_{1/2}$  values for fragment combinations [<sup>93</sup>Sr + <sup>207</sup>Tl ( $N = 126$ )], [<sup>126</sup>Sn ( $Z = 50$ ) + <sup>174</sup>Tm], and [<sup>136</sup>Xe ( $N = 82$ ) + <sup>164</sup>Tb] are shown in Fig. 4(b). The predicted

**Table 2** Predicted half-lives of probable clusters from SHN<sup>299, 300</sup>119

Parent nuclei— <sup>299</sup> 119				Parent nuclei— <sup>300</sup> 119			
Emitted cluster (MeV)	Daughter nuclei	<i>Q</i> value (MeV)	<i>T</i> <sub>1/2</sub> (s)	Emitted cluster	Daughter nuclei	<i>Q</i> value	<i>T</i> <sub>1/2</sub> (s)
<sup>4</sup> He	<sup>295</sup> Ts	11.47508	5.68 × 10 <sup>-3</sup>	<sup>4</sup> He	<sup>295</sup> Ts	11.39508	1.09 × 10 <sup>-2</sup>
<sup>83</sup> As	<sup>216</sup> Rn	279.1563	7.94 × 10 <sup>11</sup>	<sup>83</sup> As	<sup>217</sup> Rn	277.8003	7.14 × 10 <sup>12</sup>
<sup>84</sup> Se	<sup>215</sup> At	286.9447	2.21 × 10 <sup>9</sup>	<sup>84</sup> Se	<sup>216</sup> At	285.4807	2.49 × 10 <sup>10</sup>
<sup>85</sup> Br	<sup>214</sup> Po	292.7850	1.68 × 10 <sup>8</sup>	<sup>85</sup> Se	<sup>215</sup> At	285.4606	1.78 × 10 <sup>10</sup>
<sup>86</sup> Se	<sup>213</sup> At	286.8232	1.29 × 10 <sup>9</sup>	<sup>86</sup> Br	<sup>214</sup> Po	291.8920	4.25 × 10 <sup>8</sup>
<sup>87</sup> Br	<sup>212</sup> Po	294.0014	6.71 × 10 <sup>6</sup>	<sup>87</sup> Br	<sup>213</sup> Po	292.3360	1.20 × 10 <sup>8</sup>
<sup>88</sup> Kr	<sup>211</sup> Bi	301.2903	1.59 × 10 <sup>4</sup>	<sup>88</sup> Kr	<sup>212</sup> Bi	299.5992	3.25 × 10 <sup>5</sup>
<sup>89</sup> Kr	<sup>210</sup> Bi	301.0677	1.62 × 10 <sup>4</sup>	<sup>89</sup> Kr	<sup>211</sup> Bi	300.1848	6.35 × 10 <sup>4</sup>
<sup>90</sup> Kr	<sup>209</sup> Bi	302.9579	1.66 × 10 <sup>2</sup>	<sup>90</sup> Kr	<sup>210</sup> Bi	301.5412	2.27 × 10 <sup>3</sup>
<sup>91</sup> Rb	<sup>208</sup> Pb	309.2335	1.41 × 10 <sup>0</sup>	<sup>91</sup> Rb	<sup>209</sup> Pb	307.1496	9.74 × 10 <sup>1</sup>
<sup>92</sup> Sr	<sup>207</sup> Tl	313.6410	5.60 × 10 <sup>-1</sup>	<sup>92</sup> Rb	<sup>208</sup> Pb	308.3105	4.13 × 10 <sup>0</sup>
<sup>93</sup> Sr	<sup>206</sup> Tl	312.0793	1.22 × 10 <sup>1</sup>	<sup>93</sup> Sr	<sup>207</sup> Tl	312.9100	1.04 × 10 <sup>0</sup>
<sup>94</sup> Sr	<sup>205</sup> Tl	312.4065	3.59 × 10 <sup>0</sup>	<sup>94</sup> Sr	<sup>206</sup> Tl	312.8890	6.51 × 10 <sup>-1</sup>
<sup>95</sup> Y	<sup>204</sup> Hg	315.6381	1.20 × 10 <sup>1</sup>	<sup>95</sup> Sr	<sup>205</sup> Tl	310.7278	5.81 × 10 <sup>1</sup>
<sup>96</sup> Sr	<sup>203</sup> Tl	308.4193	9.49 × 10 <sup>3</sup>	<sup>96</sup> Y	<sup>204</sup> Hg	314.8101	2.82 × 10 <sup>1</sup>
<sup>97</sup> Y	<sup>202</sup> Hg	313.2003	1.02 × 10 <sup>3</sup>	<sup>97</sup> Y	<sup>203</sup> Hg	313.1742	6.47 × 10 <sup>2</sup>
<sup>98</sup> Zr	<sup>201</sup> Au	317.423	2.30 × 10 <sup>2</sup>	<sup>98</sup> Zr	<sup>202</sup> Au	317.4250	1.36 × 10 <sup>2</sup>
<sup>99</sup> Y	<sup>200</sup> Hg	309.8873	4.96 × 10 <sup>5</sup>	<sup>99</sup> Zr	<sup>201</sup> Au	315.8080	2.86 × 10 <sup>3</sup>
<sup>100</sup> Zr	<sup>199</sup> Au	315.2068	1.18 × 10 <sup>4</sup>	<sup>100</sup> Zr	<sup>200</sup> Au	315.4030	4.73 × 10 <sup>3</sup>
<sup>101</sup> Nb	<sup>198</sup> Pt	318.5350	1.11 × 10 <sup>4</sup>	<sup>101</sup> Zr	<sup>199</sup> Au	314.0448	5.72 × 10 <sup>4</sup>
<sup>102</sup> Mo	<sup>197</sup> Ir	321.565	1.26 × 10 <sup>4</sup>	<sup>102</sup> Nb	<sup>198</sup> Pt	317.9923	1.50 × 10 <sup>4</sup>
<sup>103</sup> Nb	<sup>196</sup> Pt	317.4135	6.01 × 10 <sup>4</sup>	<sup>103</sup> Nb	<sup>197</sup> Pt	317.2388	5.23 × 10 <sup>4</sup>
<sup>104</sup> Mo	<sup>195</sup> Ir	321.7763	4.50 × 10 <sup>3</sup>	<sup>104</sup> Mo	<sup>196</sup> Ir	321.5740	4.11 × 10 <sup>3</sup>
<sup>105</sup> Tc	<sup>194</sup> Os	324.4652	7.01 × 10 <sup>3</sup>	<sup>105</sup> Mo	<sup>195</sup> Ir	320.8133	1.48 × 10 <sup>4</sup>
<sup>106</sup> Mo	<sup>193</sup> Ir	320.4043	4.30 × 10 <sup>4</sup>	<sup>106</sup> Mo	<sup>194</sup> Ir	320.4498	2.36 × 10 <sup>4</sup>
<sup>107</sup> Tc	<sup>192</sup> Os	324.3723	4.90 × 10 <sup>3</sup>	<sup>107</sup> Tc	<sup>193</sup> Os	323.9344	7.24 × 10 <sup>3</sup>
<sup>108</sup> Ru	<sup>191</sup> Re	327.7510	1.26 × 10 <sup>3</sup>	<sup>108</sup> Tc	<sup>192</sup> Os	323.5953	1.12 × 10 <sup>4</sup>
<sup>109</sup> Tc	<sup>190</sup> Os	322.7308	8.54 × 10 <sup>4</sup>	<sup>109</sup> Ru	<sup>191</sup> Re	326.8780	3.51 × 10 <sup>3</sup>
<sup>110</sup> Ru	<sup>189</sup> Re	327.7920	6.89 × 10 <sup>2</sup>	<sup>110</sup> Ru	<sup>190</sup> Re	327.4460	8.35 × 10 <sup>2</sup>
<sup>111</sup> Rh	<sup>188</sup> W	330.7120	3.13 × 10 <sup>2</sup>	<sup>111</sup> Ru	<sup>189</sup> Re	326.5540	4.15 × 10 <sup>3</sup>
<sup>112</sup> Ru	<sup>187</sup> Re	326.5875	5.15 × 10 <sup>3</sup>	<sup>112</sup> Rh	<sup>188</sup> W	330.1880	4.29 × 10 <sup>2</sup>
<sup>113</sup> Rh	<sup>186</sup> W	331.0156	1.02 × 10 <sup>2</sup>	<sup>113</sup> Rh	<sup>187</sup> W	330.4610	1.90 × 10 <sup>2</sup>
<sup>114</sup> Pd	<sup>185</sup> Ta	334.6240	7.46 × 10 <sup>0</sup>	<sup>114</sup> Pd	<sup>186</sup> Ta	333.8900	2.03 × 10 <sup>1</sup>
<sup>115</sup> Ag	<sup>184</sup> Hf	336.2230	2.54 × 10 <sup>1</sup>	<sup>115</sup> Pd	<sup>185</sup> Ta	333.6100	2.89 × 10 <sup>1</sup>
<sup>116</sup> Pd	<sup>183</sup> Ta	334.8645	2.79 × 10 <sup>0</sup>	<sup>116</sup> Pd	<sup>184</sup> Ta	334.4600	3.75 × 10 <sup>0</sup>
<sup>117</sup> Ag	<sup>182</sup> Hf	337.9720	3.95 × 10 <sup>-1</sup>	<sup>117</sup> Ag	<sup>183</sup> Hf	337.2520	1.05 × 10 <sup>0</sup>
<sup>118</sup> Cd	<sup>181</sup> Lu	341.242	2.62 × 10 <sup>-2</sup>	<sup>118</sup> Ag	<sup>182</sup> Hf	337.3938	6.15 × 10 <sup>-1</sup>
<sup>119</sup> Ag	<sup>180</sup> Hf	338.1655	1.66 × 10 <sup>-1</sup>	<sup>119</sup> Ag	<sup>181</sup> Hf	337.8390	1.87 × 10 <sup>-1</sup>
<sup>120</sup> Cd	<sup>179</sup> Lu	342.7560	5.62 × 10 <sup>-4</sup>	<sup>120</sup> Cd	<sup>180</sup> Lu	342.4270	6.27 × 10 <sup>-4</sup>
<sup>121</sup> In	<sup>178</sup> Yb	345.2520	1.34 × 10 <sup>-4</sup>	<sup>121</sup> Cd	<sup>179</sup> Lu	341.9228	1.57 × 10 <sup>-3</sup>
<sup>122</sup> Cd	<sup>177</sup> Lu	342.7363	3.72 × 10 <sup>-4</sup>	<sup>122</sup> Cd	<sup>178</sup> Lu	342.7403	1.90 × 10 <sup>-4</sup>
<sup>123</sup> In	<sup>176</sup> Yb	346.6603	3.07 × 10 <sup>-6</sup>	<sup>123</sup> In	<sup>177</sup> Yb	346.2054	4.54 × 10 <sup>-6</sup>
<sup>124</sup> Sn	<sup>175</sup> Tm	350.2815	2.82 × 10 <sup>-8</sup>	<sup>124</sup> Sn	<sup>176</sup> Tm	349.3915	1.25 × 10 <sup>-7</sup>
<sup>125</sup> In	<sup>174</sup> Yb	347.0968	6.58 × 10 <sup>-7</sup>	<sup>125</sup> Sn	<sup>175</sup> Tm	349.9937	2.09 × 10 <sup>-8</sup>
<sup>126</sup> Sn	<sup>173</sup> Tm	352.0110	1.55 × 10 <sup>-10</sup>	<sup>126</sup> Sn	<sup>174</sup> Tm	351.6650	1.67 × 10 <sup>-10</sup>
<sup>127</sup> Sb	<sup>172</sup> Er	352.9210	1.06 × 10 <sup>-9</sup>	<sup>127</sup> Sn	<sup>173</sup> Tm	351.5160	1.92 × 10 <sup>-10</sup>
<sup>128</sup> Sn	<sup>171</sup> Tm	352.3113	3.66 × 10 <sup>-11</sup>	<sup>128</sup> Sn	<sup>172</sup> Tm	352.5250	7.42 × 10 <sup>-12</sup>

**Table 2** (continued)

Parent nuclei— <sup>299</sup> 119				Parent nuclei— <sup>300</sup> 119			
Emitted cluster (MeV)	Daughter nuclei	Q value (MeV)	T <sub>1/2</sub> (s)	Emitted cluster	Daughter nuclei	Q value	T <sub>1/2</sub> (s)
<sup>129</sup> Sb	<sup>170</sup> Er	354.4765	8.05 × 10 <sup>-12</sup>	<sup>129</sup> Sb	<sup>171</sup> Er	354.1368	8.24 × 10 <sup>-12</sup>
<sup>130</sup> Te	<sup>169</sup> Ho	355.8890	8.95 × 10 <sup>-12</sup>	<sup>130</sup> Sb	<sup>170</sup> Er	354.1835	5.52 × 10 <sup>-12</sup>
<sup>131</sup> Sb	<sup>168</sup> Er	354.7106	2.54 × 10 <sup>-12</sup>	<sup>131</sup> Sb	<sup>169</sup> Er	354.6926	1.17 × 10 <sup>-12</sup>
<sup>132</sup> Te	<sup>167</sup> Ho	357.2070	2.33 × 10 <sup>-13</sup>	<sup>132</sup> Te	<sup>168</sup> Ho	357.0380	1.92 × 10 <sup>-13</sup>
<sup>133</sup> I	<sup>166</sup> Dy	358.1815	3.57 × 10 <sup>-13</sup>	<sup>133</sup> Te	<sup>167</sup> Ho	357.0061	1.83 × 10 <sup>-13</sup>
<sup>134</sup> Te	<sup>165</sup> Ho	357.1718	1.98 × 10 <sup>-13</sup>	<sup>134</sup> Te	<sup>166</sup> Ho	357.3941	1.17 × 10 <sup>-13</sup>
<sup>135</sup> Xe	<sup>164</sup> Tb	358.2580	4.27 × 10 <sup>-12</sup>	<sup>135</sup> Xe	<sup>165</sup> Tb	358.7918	3.91 × 10 <sup>-13</sup>
<sup>136</sup> Xe	<sup>163</sup> Tb	360.7652	2.47 × 10 <sup>-14</sup>	<sup>136</sup> Xe	<sup>164</sup> Tb	360.3242	3.03 × 10 <sup>-14</sup>
<sup>137</sup> Cs	<sup>162</sup> Gd	360.5668	9.09 × 10 <sup>-14</sup>	<sup>137</sup> Xe	<sup>163</sup> Tb	358.7694	3.03 × 10 <sup>-13</sup>
<sup>138</sup> Ba	<sup>161</sup> Eu	359.7938	4.24 × 10 <sup>-12</sup>	<sup>138</sup> Cs	<sup>162</sup> Gd	358.9580	2.02 × 10 <sup>-12</sup>
<sup>139</sup> Cs	<sup>160</sup> Gd	358.3831	2.29 × 10 <sup>-11</sup>	<sup>139</sup> Cs	<sup>161</sup> Gd	357.9971	2.60 × 10 <sup>-11</sup>
<sup>140</sup> Ba	<sup>159</sup> Eu	359.0510	2.54 × 10 <sup>-11</sup>	<sup>140</sup> Ba	<sup>160</sup> Eu	358.5514	3.91 × 10 <sup>-11</sup>
<sup>141</sup> La	<sup>158</sup> Sm	357.9220	1.86 × 10 <sup>-9</sup>	<sup>141</sup> Ba	<sup>159</sup> Eu	357.5650	4.86 × 10 <sup>-10</sup>
<sup>142</sup> Ba	<sup>157</sup> Eu	357.0410	4.02 × 10 <sup>-9</sup>	<sup>142</sup> Ba	<sup>158</sup> Eu	356.9025	2.46 × 10 <sup>-9</sup>
<sup>143</sup> La	<sup>156</sup> Sm	357.2720	8.18 × 10 <sup>-9</sup>	<sup>143</sup> La	<sup>157</sup> Sm	356.6390	1.73 × 10 <sup>-8</sup>
<sup>144</sup> Ce	<sup>155</sup> Pm	357.1119	2.77 × 10 <sup>-8</sup>	<sup>144</sup> La	<sup>156</sup> Sm	356.0010	7.74 × 10 <sup>-8</sup>
<sup>145</sup> La	<sup>154</sup> Sm	355.0306	1.60 × 10 <sup>-6</sup>	<sup>145</sup> Ce	<sup>155</sup> Pm	355.8000	2.81 × 10 <sup>-7</sup>
<sup>146</sup> Ce	<sup>153</sup> Pm	356.0140	3.55 × 10 <sup>-7</sup>	<sup>146</sup> Ce	<sup>154</sup> Pm	355.6830	3.58 × 10 <sup>-7</sup>
<sup>147</sup> Pr	<sup>152</sup> Nd	355.3340	2.56 × 10 <sup>-6</sup>	<sup>147</sup> Ce	<sup>153</sup> Pm	354.4520	6.17 × 10 <sup>-6</sup>
<sup>148</sup> Nd	<sup>151</sup> Pr	353.9281	6.17 × 10 <sup>-5</sup>	<sup>148</sup> Pr	<sup>152</sup> Nd	354.4750	8.60 × 10 <sup>-6</sup>
<sup>149</sup> Pr	<sup>150</sup> Nd	354.4590	1.85 × 10 <sup>-5</sup>	<sup>149</sup> Pr	<sup>151</sup> Nd	353.7722	4.21 × 10 <sup>-5</sup>
				<sup>150</sup> Pr	<sup>150</sup> Nd	353.7710	4.21 × 10 <sup>-5</sup>

**Table 3** Comparison of half-lives computed by the MGLDM and the values reported by Poenaru et al. [35]. The Q values were taken from Ref. [35]

Parent nuclei	Probable cluster	Daughter nuclei	Q value (MeV)	T <sub>1/2</sub> <sup>cluster</sup> (s)	
				MGLDM	Poenaru
<sup>297</sup> 119	<sup>89</sup> Rb	<sup>208</sup> Pb (N = 126)	311.65	4.06 × 10 <sup>-2</sup>	1.95 × 10 <sup>-2</sup>
<sup>299</sup> 119	<sup>91</sup> Rb	<sup>208</sup> Pb (N = 126)	310.63	4.27 × 10 <sup>-2</sup>	3.02 × 10 <sup>-2</sup>
<sup>300</sup> 119	<sup>92</sup> Rb	<sup>208</sup> Pb (N = 126)	309.74	1.21 × 10 <sup>1</sup>	3.63 × 10 <sup>1</sup>

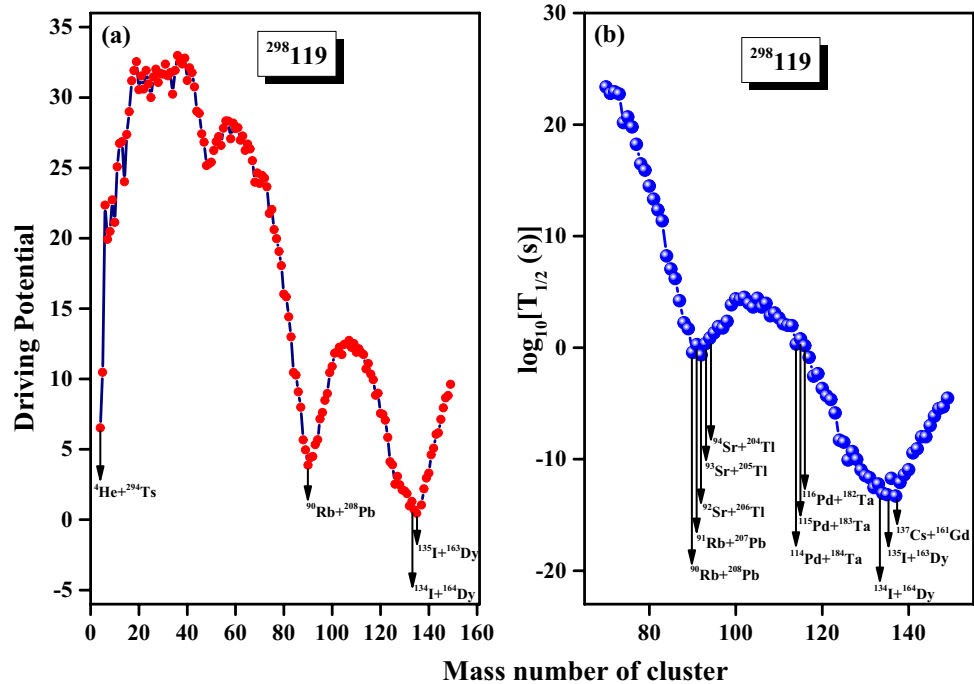
heavy cluster or its residual nuclei are extremely stable because of the closed-shell effect, which is one of the distinctive characteristics of heavy-particle radioactivity.

The probabilities of cluster emissions from each isotope of <sup>297–300</sup>119 with a half-life similar to that of the α-decay half-life are listed in Table 4. Columns 1–4 show the parent nuclei, probable clusters, daughter nuclei, and Q values, respectively. Columns 5 and 6 represent the heavy-cluster half-life and α-decay half-life from each isotope of <sup>297–300</sup>119, respectively. If the predicted heavy-cluster half-life is close to the α-decay half-life, then there is a chance that the SHN will go through heavy-cluster decay. Various isotopes of indium (Z = 49), cadmium (Z = 48), and palladium (Z = 46), which have proton numbers close to magic number Z = 50, are the principal heavy clusters with half-lives equivalent to the α half-life, as predicted from the SHN

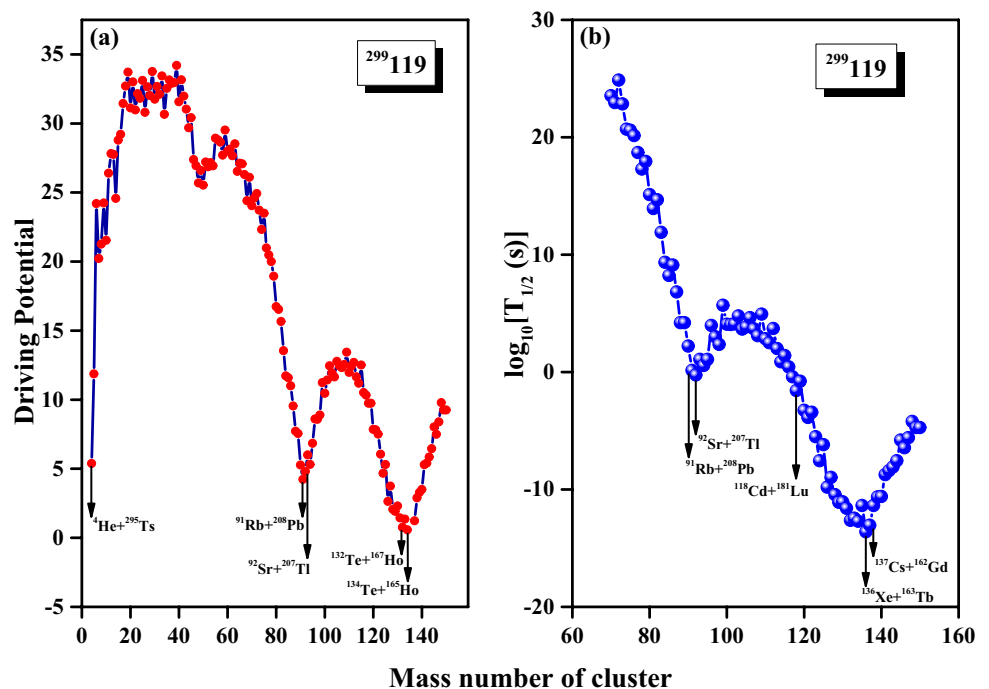
of <sup>297–300</sup>119 and listed in Table 4. Another probable decay mechanism involved the different isotopes of rubidium leading to daughter nuclei of lead (Z = 82), strontium leading to thallium (Z = 81), and krypton leading to bismuth (Z = 83). In all these cases, the proton number and number of neutrons in the residual nuclei were near the magic numbers (Z = 82, N = 126). This clearly illustrates the role played by the magic numbers in radioactive decay. Detecting these decays with T<sub>1/2</sub> values comparable to that of the α decay will be beneficial for future studies.

Table 5 lists the possible cluster–daughter combinations with the minimum half-life values among all the fragmentations of each isotope of <sup>297–300</sup>119. When the half-life was low, the decay probabilities increased. From the table, it can be deduced that the most probable clusters with the lowest half-lives were various isotopes of Cs, Xe, and I, with

**Fig. 2** **a** Plot of driving potential vs. mass number of clusters for <sup>298</sup>119 for touching configuration  $r = C_1 + C_2$ . **b** Variation of logarithm of half-life with mass number of clusters for probable heavy-cluster decay from <sup>298</sup>119



**Fig. 3** **a** Plot of driving potential vs. mass number of clusters for <sup>299</sup>119 for touching configuration  $r = C_1 + C_2$ . **b** Variation of logarithm of half-life with mass number of clusters for probable heavy-cluster decay from <sup>299</sup>119



neutron number  $N = 82$  or near it. Consequently, we could identify an area where HPR dominated the  $\alpha$  decay in this study and all the possible heavy clusters had the magic number of neutrons ( $N = 82$ ) or close to it, as listed in Table 5. This study revealed that the likelihood of decay increases when either the emitted cluster or daughter nucleus possesses stable configurations characterized by the magic number of protons or neutrons. Therefore, our study demonstrated the significance of the shell effect on nuclear decay.

Furthermore, calculations were performed to determine the yield of every possible decay combination from <sup>297–300</sup>119. Yield  $Y$  for a decay combination is computed as follows:

$$Y = \frac{P}{\sum P} \times 100\%, \quad (11)$$

**Fig. 4** **a** Plot of driving potential vs. mass number of clusters for  $^{300}_{119}$  for touching configuration  $r = C_1 + C_2$ . **b** Variation of logarithm of half-life with mass number of clusters for probable heavy-cluster decay from  $^{300}_{119}$

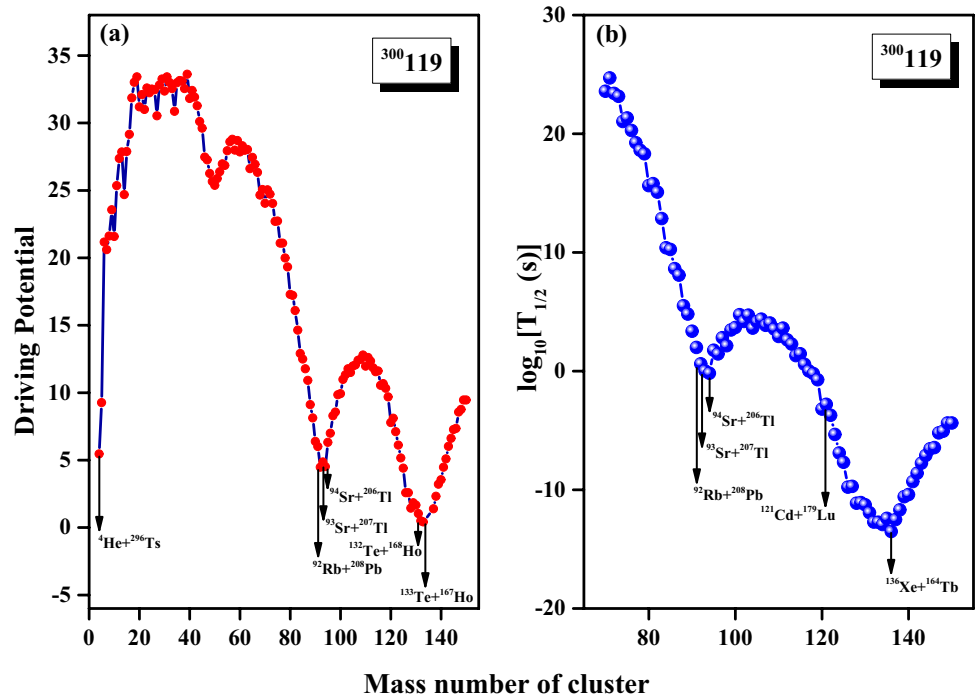


**Table 4** Possible HPR from  $^{297-300}_{119}$  SHN with half-life comparable to that of  $\alpha$ -decay half-life

Parent nuclei	Probable cluster	Daughter nuclei	$Q$ value (MeV)	$T_{1/2}^{\text{cluster}}$ (s)	$T_{1/2}^{\alpha}$ (s)
$^{297}_{119}$	$^{116}\text{Pd}$ ( $N=70$ )	$^{181}\text{Ta}$ ( $N=108$ )	335.5901	$1.86 \times 10^0$	$2.76 \times 10^0$
	$^{88}\text{Kr}$ ( $N=52$ )	$^{209}\text{Bi}$ ( $N=126$ )	305.2699	$7.13 \times 10^0$	
	$^{90}\text{Rb}$ ( $N=53$ )	$^{207}\text{Pb}$ ( $N=125$ )	309.1380	$9.33 \times 10^0$	
$^{298}_{119}$	$^{116}\text{Pd}$ ( $N=70$ )	$^{182}\text{Ta}$ ( $N=109$ )	335.4217	$1.50 \times 10^0$	$7.89 \times 10^0$
	$^{115}\text{Pd}$ ( $N=69$ )	$^{183}\text{Ta}$ ( $N=110$ )	334.8795	$6.00 \times 10^0$	
	$^{114}\text{Pd}$ ( $N=68$ )	$^{184}\text{Ta}$ ( $N=111$ )	335.4890	$2.08 \times 10^0$	
	$^{94}\text{Sr}$ ( $N=56$ )	$^{204}\text{Tl}$ ( $N=123$ )	312.3518	$7.13 \times 10^0$	
	$^{93}\text{Sr}$ ( $N=55$ )	$^{205}\text{Tl}$ ( $N=124$ )	313.0668	$2.26 \times 10^0$	
	$^{91}\text{Rb}$ ( $N=54$ )	$^{207}\text{Pb}$ ( $N=125$ )	309.3570	$1.88 \times 10^0$	
$^{299}_{119}$	$^{120}\text{Cd}$ ( $N=72$ )	$^{179}\text{Lu}$ ( $N=108$ )	342.7560	$5.62 \times 10^{-4}$	$5.68 \times 10^{-3}$
	$^{121}\text{In}$ ( $N=72$ )	$^{178}\text{Yb}$ ( $N=108$ )	345.2520	$1.34 \times 10^{-4}$	
	$^{122}\text{Cd}$ ( $N=74$ )	$^{177}\text{Lu}$ ( $N=106$ )	342.7363	$3.72 \times 10^{-4}$	
$^{300}_{119}$	$^{121}\text{Cd}$ ( $N=73$ )	$^{179}\text{Lu}$ ( $N=108$ )	341.9228	$1.57 \times 10^{-3}$	$1.09 \times 10^{-2}$

**Table 5** Most probable heavy-cluster decay from  $^{297-300}_{119}$  SHN with least half-life among all splitting

Parent nuclei	Probable cluster	Daughter nuclei	$Q$ value (MeV)	$T_{1/2}^{\text{cluster}}$ (s)
$^{297}_{119}$	$^{137}\text{Cs}$ ( $N=82$ )	$^{160}\text{Gd}$ ( $N=96$ )	361.8079	$3.05 \times 10^{-14}$
	$^{136}\text{Xe}$ ( $N=82$ )	$^{161}\text{Tb}$ ( $N=96$ )	361.2110	$2.47 \times 10^{-14}$
$^{298}_{119}$	$^{137}\text{Cs}$ ( $N=82$ )	$^{161}\text{Gd}$ ( $N=97$ )	361.2119	$4.91 \times 10^{-14}$
	$^{135}\text{I}$ ( $N=82$ )	$^{163}\text{Dy}$ ( $N=97$ )	359.3201	$6.44 \times 10^{-14}$
	$^{134}\text{I}$ ( $N=81$ )	$^{164}\text{Dy}$ ( $N=98$ )	359.1706	$8.65 \times 10^{-14}$
$^{299}_{119}$	$^{137}\text{Cs}$ ( $N=82$ )	$^{162}\text{Gd}$ ( $N=98$ )	360.5668	$9.09 \times 10^{-14}$
	$^{136}\text{Xe}$ ( $N=82$ )	$^{163}\text{Tb}$ ( $N=98$ )	360.7652	$2.47 \times 10^{-14}$
$^{300}_{119}$	$^{136}\text{Xe}$ ( $N=82$ )	$^{164}\text{Tb}$ ( $N=99$ )	360.3242	$3.03 \times 10^{-14}$

where  $P$  is the barrier penetrability for the decay, and  $\sum P$  is the sum of the barrier penetrabilities of all the combinations. Tunneling possibility  $P$  was given by Eq. (6) in Sect. 2. Table 6 presents the tabulated data for the decay combinations that exhibited the highest yield values.

Once the yield was calculated, the logarithmic yield was plotted against the mass number of clusters in each case. Figures 5, 6, 7, and 8 show the plots of  $\log_{10}[Y]$  versus the number of clusters for all the decay combinations involving clusters with mass numbers ranging from 80 to 150 for  $^{297}119$ ,  $^{298}119$ ,  $^{299}119$ , and  $^{300}119$ , respectively. From all the graphs, it can be observed that the logarithm of the yield reached its maximum at two distinct positions. One peak was located in the vicinity of clusters with mass numbers ranging from 88 to 94, while the other peak was found around the clusters having  $132 \leq A \leq 138$ . For  $^{297}119$ , the first maximum occurred when the isotope decayed into cluster  $^{89}\text{Rb}$ , resulting in the formation of doubly magic daughter nuclei,  $^{208}\text{Pb}$  ( $Z = 82$ ,  $N = 126$ ). The second maximum, which had the highest  $\log_{10}[Y]$  value among all the decay combinations, occurred for the combination [ $^{136}\text{Xe} + ^{161}\text{Tb}$ ]. This was also the reaction with the minimum driving potential in the cold valley plot of  $^{297}119$ ,

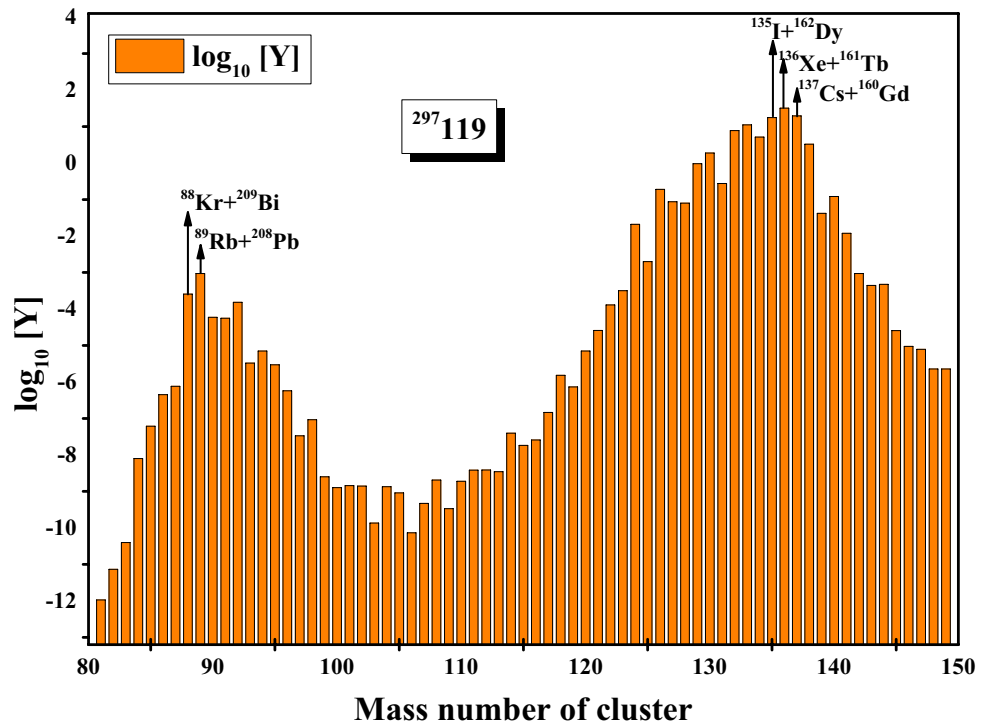
making it the most probable decay. The first peak in the yield for the cluster emissions from  $^{298}119$  and  $^{299}119$  was achieved when the daughter nuclei,  $^{208}\text{Pb}$ , were formed, with the respective clusters generated being  $^{90}\text{Rb}$  and  $^{91}\text{Rb}$ . The second maximum yield value was achieved in the cases of  $^{298}119$  with combination [ $^{135}\text{I}$  ( $N = 82$ ) +  $^{163}\text{Dy}$ ] and  $^{299}119$  with combination [ $^{136}\text{Xe}$  ( $N = 82$ ) +  $^{163}\text{Tb}$ ]. For  $^{300}119$ , the first and second yield peaks occurred for decay combinations [ $^{94}\text{Sr} + ^{206}\text{Tl}$  ( $N = 125$ )] and [ $^{136}\text{Xe}$  ( $N = 82$ ) +  $^{164}\text{Tb}$ ], respectively. Based on these observations, we can infer that if the cluster or daughter nuclei involved in the decay possess a magic number of neutrons, the probability of the reaction occurring is higher, leading to an increased yield for that specific decay combination. Magic numbers are known to provide greater stability to atomic nuclei, and their presence in decay products enhances the probability of decay combinations.

Table 7 lists the decay modes of  $^{297-300}119$ , which were determined by comparing the  $T_{1/2}$  values of the  $\alpha$  decay with the  $T_{1/2}$  values of the spontaneous fission. Columns 1–4 indicate the parent nuclei,  $Q$  values, SF half-lives, and  $\alpha$ -decay half-lives, respectively. The mass inertia-dependent

**Table 6** Table showing some of the maximum  $\log_{10}[Y]$  values for different decay combinations from  $^{297-300}119$

Parent nuclei	Cluster nuclei	Daughter nuclei	$Q$ value (MeV)	Penetrability $P$	$\log_{10}[Y]$
$^{297}119$	$^{88}\text{Kr}$	$^{209}\text{Bi}$ ( $N = 126$ )	305.2699	$6.49 \times 10^{-6}$	-3.592
	$^{89}\text{Rb}$	$^{208}\text{Pb}$ ( $N = 126$ )	310.7805	$2.38 \times 10^{-5}$	-3.028
	$^{90}\text{Rb}$	$^{207}\text{Pb}$ ( $N = 125$ )	309.1380	$1.50 \times 10^{-6}$	-4.228
	$^{135}\text{I}$ ( $N = 82$ )	$^{162}\text{Dy}$	359.2804	$4.47 \times 10^{-1}$	1.246
	$^{136}\text{Xe}$ ( $N = 82$ )	$^{161}\text{Tb}$	361.2110	$8.10 \times 10^{-1}$	1.503
	$^{137}\text{Cs}$ ( $N = 82$ )	$^{160}\text{Gd}$	361.8079	$4.97 \times 10^{-1}$	1.291
	$^{298}119$	$^{90}\text{Rb}$	$^{208}\text{Pb}$ ( $N = 126$ )	310.2745	$2.68 \times 10^{-5}$
$^{91}\text{Rb}$		$^{207}\text{Pb}$ ( $N = 125$ )	309.3570	$6.95 \times 10^{-6}$	-3.584
$^{92}\text{Sr}$		$^{206}\text{Tl}$ ( $N = 125$ )	314.2803	$1.20 \times 10^{-5}$	-3.346
$^{134}\text{I}$ ( $N = 81$ )		$^{164}\text{Dy}$	359.1706	$5.97 \times 10^{-1}$	1.349
$^{135}\text{I}$ ( $N = 82$ )		$^{163}\text{Dy}$	359.3201	$7.49 \times 10^{-1}$	1.448
$^{137}\text{Cs}$ ( $N = 82$ )		$^{161}\text{Gd}$	361.2119	$4.08 \times 10^{-1}$	1.184
$^{299}119$		$^{91}\text{Rb}$	$^{208}\text{Pb}$ ( $N = 126$ )	309.2335	$9.65 \times 10^{-6}$
	$^{92}\text{Sr}$	$^{207}\text{Tl}$ ( $N = 126$ )	313.6410	$5.88 \times 10^{-6}$	-3.712
	$^{93}\text{Sr}$	$^{206}\text{Tl}$ ( $N = 125$ )	312.0793	$4.50 \times 10^{-7}$	-4.828
	$^{132}\text{Te}$ ( $N = 80$ )	$^{167}\text{Ho}$	357.2070	$5.46 \times 10^{-1}$	1.256
	$^{134}\text{Te}$ ( $N = 82$ )	$^{165}\text{Ho}$	357.1718	$6.54 \times 10^{-1}$	1.334
	$^{136}\text{Xe}$ ( $N = 82$ )	$^{163}\text{Tb}$	360.7652	$9.98 \times 10^{-1}$	1.518
	$^{137}\text{Cs}$ ( $N = 82$ )	$^{162}\text{Gd}$	360.5668	$2.97 \times 10^{-1}$	0.992
$^{300}119$	$^{92}\text{Rb}$	$^{208}\text{Pb}$ ( $N = 126$ )	308.3105	$4.39 \times 10^{-6}$	-4.011
	$^{93}\text{Sr}$	$^{207}\text{Tl}$ ( $N = 126$ )	312.9100	$4.02 \times 10^{-6}$	-4.049
	$^{94}\text{Sr}$	$^{206}\text{Tl}$ ( $N = 125$ )	312.8890	$6.47 \times 10^{-6}$	-3.843
	$^{132}\text{Te}$ ( $N = 80$ )	$^{168}\text{Ho}$	357.0380	$7.13 \times 10^{-1}$	1.199
	$^{133}\text{Te}$ ( $N = 81$ )	$^{167}\text{Ho}$	357.0061	$7.61 \times 10^{-1}$	1.227
	$^{134}\text{Te}$ ( $N = 82$ )	$^{166}\text{Ho}$	357.3941	$9.96 \times 10^{-1}$	1.344
	$^{136}\text{Xe}$ ( $N = 82$ )	$^{164}\text{Tb}$	360.3242	$9.98 \times 10^{-1}$	1.345

**Fig. 5** (Color online) Plot showing  $\log_{10}[Y]$  vs. mass number of clusters for all the possible decay combinations from  $^{297}_{119}$



**Fig. 6** (Color online) Plot showing  $\log_{10}[Y]$  vs. mass number of clusters for all the possible decay combinations from  $^{298}_{119}$

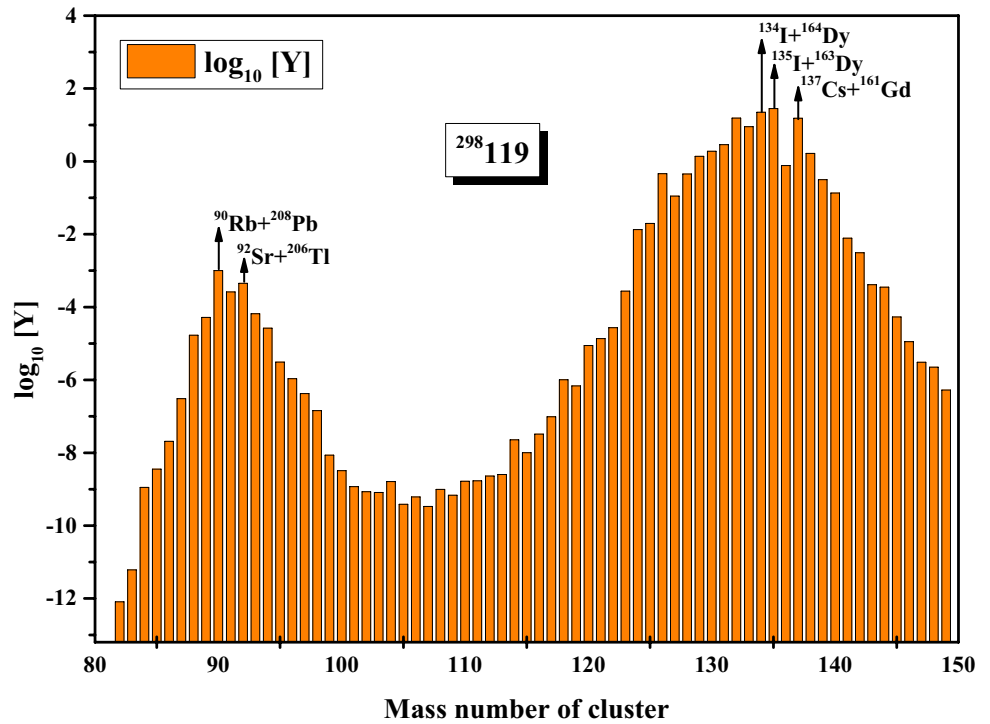


**Fig. 7** (Color online) Plot showing  $\log_{10}[Y]$  vs. mass number of clusters for all the possible decay combinations from  $^{299}119$

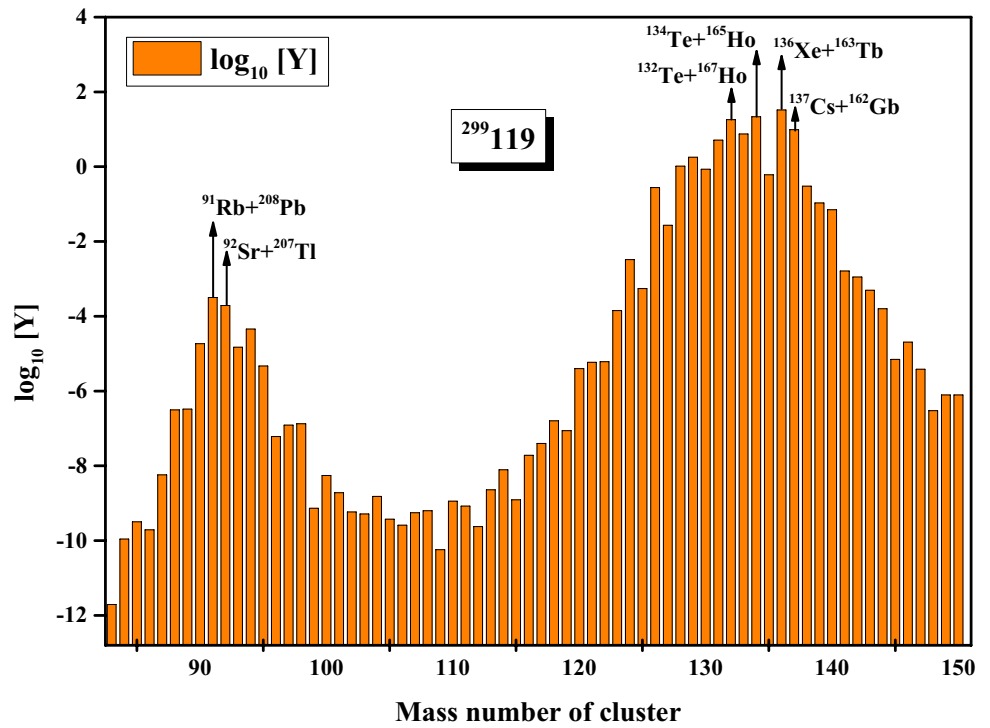


**Fig. 8** (Color online) Plot showing  $\log_{10}[Y]$  vs. mass number of clusters for all the possible decay combinations from  $^{300}119$

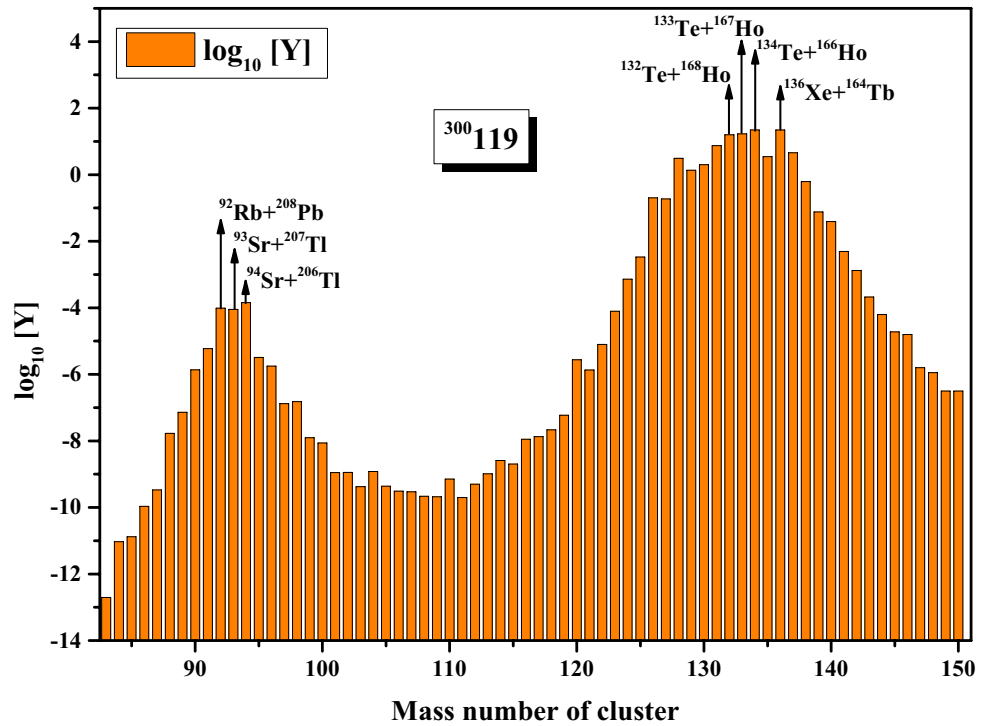


**Table 7** Decay modes of  $^{297-300}_{119}$  isotopes

Parent nuclei	$Q$ value (MeV)	$T_{1/2}^{SF}$ (s)	$T_{1/2}^{\alpha}$ (s)	$T_{1/2}^{Expt.}$ (s)[39]	Mode of decay	
					Theory	Expt. [39]
$^{297}_{119}$	10.46508	$2.12 \times 10^{+09}$	$2.76 \times 10^{+00}$		$\alpha$	
$^{293}_{Ts}$	11.32508	$2.87 \times 10^{+09}$	$3.80 \times 10^{-03}$	$2.20 \times 10^{-02}$	$\alpha$	$\alpha$
$^{289}_{Mc}$	10.48508	$2.39 \times 10^{+07}$	$1.41 \times 10^{-01}$	$3.30 \times 10^{-01}$	$\alpha$	$\alpha$
$^{285}_{Nh}$	10.01508	$1.60 \times 10^{+03}$	$6.87 \times 10^{-01}$	$4.20 \times 10^{+00}$	$\alpha$	$\alpha$
$^{281}_{Rg}$	9.89508	$3.33 \times 10^{-02}$	$3.48 \times 10^{-01}$	$1.70 \times 10^{+01}$	SF	SF
$^{277}_{Mt}$	9.90508	$1.04 \times 10^{-03}$	$7.49 \times 10^{-02}$	$5.00 \times 10^{-03}$	SF	SF
$^{298}_{119}$	10.33508	$1.68 \times 10^{+12}$	$7.89 \times 10^{+00}$		$\alpha$	
$^{294}_{Ts}$	11.18508	$2.56 \times 10^{+13}$	$1.03 \times 10^{-02}$	$5.10 \times 10^{-02}$	$\alpha$	$\alpha$
$^{290}_{Mc}$	10.40508	$2.41 \times 10^{+11}$	$2.85 \times 10^{-01}$	$6.50 \times 10^{-01}$	$\alpha$	$\alpha$
$^{286}_{Nh}$	9.79508	$3.36 \times 10^{+07}$	$3.67 \times 10^{+00}$	$9.50 \times 10^{+00}$	$\alpha$	$\alpha$
$^{282}_{Rg}$	9.54508	$5.60 \times 10^{+02}$	$4.58 \times 10^{+00}$	$1.00 \times 10^{+02}$	$\alpha$	$\alpha$
$^{278}_{Mt}$	9.58508	$1.61 \times 10^{+00}$	$7.66 \times 10^{-01}$	$4.50 \times 10^{+00}$	$\alpha$	$\alpha$
$^{274}_{Bh}$	8.93508	$1.50 \times 10^{+02}$	$1.67 \times 10^{+01}$	$4.40 \times 10^{+01}$	$\alpha$	$\alpha$
$^{299}_{119}$	11.47508	$1.93 \times 10^{+08}$	$5.68 \times 10^{-03}$		$\alpha$	
$^{295}_{Ts}$	9.23508	$8.17 \times 10^{+09}$	$3.55 \times 10^{+03}$		$\alpha$	
$^{291}_{Mc}$	10.29508	$9.54 \times 10^{+08}$	$4.36 \times 10^{-01}$		$\alpha$	
$^{287}_{Nh}$	9.65508	$4.86 \times 10^{+04}$	$7.33 \times 10^{+00}$		$\alpha$	
$^{283}_{Rg}$	9.36508	$1.21 \times 10^{+00}$	$1.25 \times 10^{+01}$		SF	
$^{279}_{Mt}$	9.38508	$1.78 \times 10^{-03}$	$2.32 \times 10^{+00}$		SF	
$^{300}_{119}$	11.39508	$1.83 \times 10^{+11}$	$1.09 \times 10^{-02}$		$\alpha$	
$^{296}_{Ts}$	8.94508	$1.72 \times 10^{+13}$	$4.37 \times 10^{+04}$		$\alpha$	
$^{292}_{Mc}$	10.20508	$1.22 \times 10^{+13}$	$9.55 \times 10^{-01}$		$\alpha$	
$^{288}_{Nh}$	9.57508	$5.89 \times 10^{+08}$	$1.57 \times 10^{+01}$		$\alpha$	
$^{284}_{Rg}$	9.03508	$3.00 \times 10^{+04}$	$1.75 \times 10^{+02}$		$\alpha$	
$^{280}_{Mt}$	9.13508	$3.69 \times 10^{+01}$	$1.70 \times 10^{+01}$		$\alpha$	
$^{276}_{Bh}$	8.04508	$9.84 \times 10^{-01}$	$2.05 \times 10^{+04}$		SF	
$^{272}_{Db}$	7.94508	$1.70 \times 10^{+02}$	$8.72 \times 10^{+03}$		SF	

expression [26] was employed to calculate the SF half-life, while the MGLDM method was utilized to obtain the  $\alpha$ -decay half-life. The equation for the SF half-life is as follows:

$$\log_{10}[T_{1/2}(yr)] = c_1 + c_2 \left( \frac{Z^2}{(1 - kI^2)A} \right) + c_3 \left( \frac{Z^2}{(1 - kI^2)} \right)^2 + c_4 E_{shell} + c_5 I_{rigid} + h_i, \tag{12}$$

where  $I_{rigid} = B_{rigid} [1 + 0.31\beta_2 + 0.44\beta_2^2 + \dots]$  is the mass inertia of a rigid nucleus [42, 43], with mass inertia parameter  $B_{rigid} = \frac{2}{5}MR^2 = 0.0138A^{5/3} (\hbar^2/MeV)$  and  $R = 1.2A^{1/3}(\text{fm})$  M represents the mass of the nucleus, while  $\beta_2$  stands for the quadrupole deformation of the nucleus. The given constants have specific values:  $c_1 = 1208.763104$ ,  $c_2 = -49.26439288$ ,  $c_3 = 0.486222575$ ,  $c_4 = 3.557962857$ , and  $c_5 = 0.04292571494$ . Additionally, the value of  $k$  is set at 2.6

[44], and  $h_i$  represents the blocking effect for a nucleon that is unpaired. For heavy and SHN with even numbers of both protons and neutrons,  $h_i$  is set to 0. However, for nuclei with an odd number of neutrons (odd- $N$  nuclei),  $h_{eo}$  is equal to

2.749814, and for nuclei with an odd number of protons (odd- $Z$  nuclei),  $h_{oe}$  is equal to 2.490760. The experimental half-lives reported in Ref. [45] are listed in the 5th column. The theoretical and experimental decay modes are presented in columns 6 and 7, respectively. The daughter nuclei resulting from the decay of  $^{297}_{119}$ , namely  $^{293}_{Ts}$ ,  $^{289}_{Mc}$ , and  $^{285}_{Nh}$ , possess half-lives shorter than the spontaneous fission half-life. Consequently, they are capable of enduring the fission process. Spontaneous fission takes place in daughter nuclei  $^{281}_{Rg}$  and  $^{277}_{Mt}$  because their spontaneous fission half-life is shorter than their  $\alpha$  half-life.

Hence, this work implies that the decay of <sup>297</sup>119 includes four  $\alpha$  decay chains and two spontaneous fissions. The decay of parent nucleus <sup>298</sup>119 involves seven  $\alpha$  decay chains only because of the significantly shorter  $\alpha$  half-lives compared to the SF half-lives. In the context of parent nucleus <sup>299</sup>119, the  $\alpha$  half-life is shorter than the SF half-life for the initial four decays. Subsequently, for daughter nuclei <sup>283</sup>Rg and <sup>279</sup>Mt, spontaneous fission takes place due to the  $\alpha$  half-lives being longer than the SF half-lives. Consequently, the decay of <sup>299</sup>119 involves a sequence of four  $\alpha$  decay chains followed by two instances of spontaneous fission. Similarly, <sup>300</sup>119 experiences a series of six  $\alpha$  decays, followed by two occurrences of spontaneous fission. The currently obtainable experimental half-life, as well as the predicted decay mode based on the accessible experimental data, provide additional validation of our predictions. We would like to mention that the isotopes of  $Z=119$  are the most promising candidates for synthesis in the future. The present study determined the most favorable heavy cluster emissions from these nuclei and provided suitable projectile target combinations (obtained from the cold reaction valley) for their synthesis, depending on the availability and lifetimes of the projectiles and targets.

## 4 Summary

We investigated all of the possible cluster–daughter combinations for isotopes <sup>297–300</sup>119 and computed the heavy-cluster decay half-lives using the MGLDM, including the decay energy-dependent preformation probabilities. The expected half-life of any heavy cluster within experimentally detectable limits had a  $Z_C \geq 32$ , and these results were in line with the predictions of Poenaru et al. that SHN with  $Z > 110$  will produce heavy particles with penetrability comparable to or greater than that of the  $\alpha$ -decay. The isotopes of heavy clusters of Kr, Rb, Sr, Pa, In, and Cd have half-lives comparable to the  $\alpha$  half-lives; and the isotopes of clusters of I, Xe, and Cs have a minimum half-life ( $10^{-14}$  s), indicating the role of shell closure ( $Z = 82$ ,  $N = 82$ , and  $N = 126$ ) for cluster and daughter nuclei in heavy-cluster radioactivity. We anticipate that isotopes <sup>297,299</sup>119 will decay in  $4\alpha$  chains, isotope <sup>300</sup>119 will decay in  $6\alpha$  chains, and isotope <sup>298</sup>119 will decay in continuous  $\alpha$  chains. The predicted half-lives ( $\alpha$  and SF) and modes of decay of nuclei in the disintegration chains of <sup>297–300</sup>119 agree with the experimental data, which verifies the reliability of our findings.

**Acknowledgements** K.P.S. would like to thank the Council of Scientific and Industrial Research, Government of India, for their financial support under the scheme “Emeritus Scientist, CSIR,” No. 21(1154)/22/EMR-II dated 20-05-2022.

**Author contributions** All authors contributed to the study conception and design. Material preparation, data collection and analysis were performed by Megha Chandran, V.K. Anjali and K.P. Santhosh. The first draft of the manuscript was written by Megha Chandran and all authors commented on previous versions of the manuscript. All authors read and approved the final manuscript.

## Declarations

**Conflict of interest** The authors declare that they have no competing interests.

## References

1. F.G. Werner, J.A. Wheeler, Superheavy nuclei. *Phys. Rev.* **109**, 126 (1958). <https://doi.org/10.1103/PhysRev.109.126>
2. W.D. Myers, W.J. Swiatecki, Nuclear masses and deformations. *Nucl. Phys. A* **81**, 1 (1966). [https://doi.org/10.1016/0029-5582\(66\)90639-0](https://doi.org/10.1016/0029-5582(66)90639-0)
3. R.K. Gupta, S.K. Patra, W. Greiner, Structure of <sup>294,302</sup>120 nuclei using the relativistic mean-field method. *Mod. Phys. Lett. A* **12**, 1727 (1997). <https://doi.org/10.1142/S021773239700176X>
4. G.A. Lalazissis, M.M. Sharma, P. Ring et al., Superheavy nuclei in the relativistic mean-field theory. *Nucl. Phys. A* **608**, 202 (1996). [https://doi.org/10.1016/0375-9474\(96\)00273-4](https://doi.org/10.1016/0375-9474(96)00273-4)
5. S. Cwiok, J. Dobaczewski, P.H. Heenen et al., Shell structure of the superheavy elements. *Nucl. Phys. A* **611**, 211 (1996). [https://doi.org/10.1016/S0375-9474\(96\)00337-5](https://doi.org/10.1016/S0375-9474(96)00337-5)
6. K. Rutz, M. Bender, T. Bürvenich et al., Superheavy nuclei in self-consistent nuclear calculations. *Phys. Rev. C* **56**, 238 (1997). <https://doi.org/10.1103/PhysRevC.56.238>
7. M. Bender, K. Rutz, P.G. Reinhard et al., Shell structure of superheavy nuclei in self-consistent mean-field models. *Phys. Rev. C* **60**, 034304 (1999). <https://doi.org/10.1103/PhysRevC.60.034304>
8. A.T. Kruppa, M. Bender, W. Nazarewicz et al., Shell corrections of superheavy nuclei in self-consistent calculations. *Phys. Rev. C* **61**, 034313 (2000). <https://doi.org/10.1103/PhysRevC.61.034313>
9. S. Hofmann, G. Munzenberg, The discovery of the heaviest elements. *Rev. Mod. Phys.* **72**, 733 (2000). <https://doi.org/10.1103/RevModPhys.72.733>
10. Yu. Ts. Oganessian, Heaviest nuclei from <sup>48</sup>Ca-induced reactions. *J. Phys. G Nucl. Part Phys.* **34**, R165 (2007). <https://doi.org/10.1088/0954-3899/34/4/R01>
11. S. Hofman, N.S. Heinz, R. Mann et al., Review of even element super-heavy nuclei and search for element 120. *Eur. Phys. J. A* **52**, 180 (2016). <https://doi.org/10.1140/epja/i2016-16180-4>
12. J. Khuyagbaatar, A. Yakushev, C.E. Düllmann et al., Search for elements 119 and 120. *Phys. Rev. C* **102**, 064602 (2020). <https://doi.org/10.1103/PhysRevC.102.064602>
13. P.B. Price, Heavy-particle radioactivity ( $A > 4$ ). *Annu. Rev. Nucl. Part. Sci.* **39**, 19 (1989). <https://doi.org/10.1146/annurev.ns.39.120189.000315>
14. E. Hourani, M. Hussonnois, D.N. Poenaru, Radioactivities by light fragment (C, Ne, Mg) emission. *Ann. Phys. (Paris)* **14**, 311 (1989). <https://doi.org/10.1051/anphys:01989001403031100>
15. S.S. Malik, S. Singh, R.K. Puri et al., Clustering phenomena in radioactive and stable nuclei and in heavy-ion collisions. *Pramana* **32**, 419 (1989). <https://doi.org/10.1007/BF02845974>
16. D.N. Poenaru, W. Greiner, M. Ivascu et al., Heavy cluster decay of trans-zirconium “stable” nuclides. *Phys. Rev. C* **32**, 2198 (1985). <https://doi.org/10.1103/PhysRevC.32.2198>

17. G. Royer, R. Moustabchir, Light nucleus emission within a generalized liquid-drop model and quasimolecular shapes. *Nucl. Phys. A* **683**, 182 (2001). [https://doi.org/10.1016/S0375-9474\(00\)00454-1](https://doi.org/10.1016/S0375-9474(00)00454-1)
18. G. Royer, Q. Ferrier, M. Pineau, Alpha and cluster decays of superheavy elements and 2p radioactivity of medium nuclei. *Nucl. Phys. A* **1021**, 122427 (2022). <https://doi.org/10.1016/j.nuclphysa.2022.122427>
19. J. Blocki, J. Randrup, W.J. Swiatecki et al., Proximity forces. *Ann. Phys.* **105**, 427 (1977). [https://doi.org/10.1016/0003-4916\(77\)90249-4](https://doi.org/10.1016/0003-4916(77)90249-4)
20. G. Royer, B.J. Remaud, Fission processes through compact and creviced Shapes. *J. Phys. G Nucl. Part Phys.* **10**, 1057 (1984). <https://doi.org/10.1088/0305-4616/10/8/011>
21. G. Royer, B.J. Remaud, Static and dynamic fusion barriers in heavy-ion reactions. *Nucl. Phys. A* **444**, 477 (1985). [https://doi.org/10.1016/0375-9474\(85\)90464-6](https://doi.org/10.1016/0375-9474(85)90464-6)
22. C. Nithya, K.P. Santhosh, Studies on the decay modes of superheavy nuclei with  $Z = 120$ . *Nucl. Phys.* **1020**, 122400 (2022). <https://doi.org/10.1016/j.nuclphysa.2022.122400>
23. D.N. Poenaru, R.A. Gherghescu, W. Greiner, Heavy-particle radioactivity of superheavy nuclei. *Phys. Rev. Lett.* **107**, 062503 (2011). <https://doi.org/10.1103/PhysRevLett.107.062503>
24. Y.L. Zhang, Y.Z. Wang, Systematic study of cluster radioactivity of superheavy nuclei. *Phys. Rev. C* **97**, 014318 (2018). <https://doi.org/10.1103/PhysRevC.97.014318>
25. K.P. Santhosh, C. Nithya, Systematic studies of  $\alpha$  and heavy-cluster emissions from superheavy nuclei. *Phys. Rev. C* **97**, 064616 (2018). <https://doi.org/10.1103/PhysRevC.97.064616>
26. K.P. Santhosh, T.A. Jose, N.K. Deepak, Radioactive decay of  $^{288-296}\text{Og}$  via heavy cluster emission within a modified generalized liquid drop model with a  $Q$ -value-dependent preformation factor. *Phys. Rev. C* **103**, 064612 (2021). <https://doi.org/10.1103/PhysRevC.103.064612>
27. K.P. Santhosh, T.A. Jose, N.K. Deepak, Probable chances of radioactive decays from superheavy nuclei  $^{290-304}120$  within a modified generalized liquid drop model with a  $Q$ -value-dependent preformation factor. *Phys. Rev. C* **105**, 054605 (2022). <https://doi.org/10.1103/PhysRevC.105.054605>
28. Y.B. Qian, Z. Ren, New look at Geiger-Nuttall law and  $\alpha$  clustering of heavy nuclei. *Chin. Phys. C* **45**, 021002 (2021). <https://doi.org/10.1088/1674-1137/abce14>
29. T. Wan, S.L. Tang, Y.B. Qian,  $\alpha$ -decay properties of superheavy nuclei with  $117 \leq Z \leq 120$  from the systematics of decay chains and isotopic chains. *Chin. Phys. C* **48**, 034103 (2024). <https://doi.org/10.1088/1674-1137/ad1582>
30. J. Blocki, W.J. Swiatecki, A generalization of the proximity force theorem. *Ann. Phys.* **132**, 53 (1981). [https://doi.org/10.1016/0003-4916\(81\)90268-2](https://doi.org/10.1016/0003-4916(81)90268-2)
31. K.P. Santhosh, T.A. Jose, Half-lives of cluster radioactivity using the modified generalized liquid drop model with a new preformation factor. *Phys. Rev. C* **99**, 064604 (2019). <https://doi.org/10.1103/PhysRevC.99.064604>
32. K.P. Santhosh, V.K. Anjali, Systematic studies on  $\alpha$  decay of Po, At, Rn, Fr and Ra using modified generalized liquid drop model. *Eur. Phys. J. A* **59**, 248 (2023). <https://doi.org/10.1140/epja/s10050-023-01164-8>
33. K.P. Santhosh, C. Nithya, H. Hassanabadi et al.,  $\alpha$ -decay half-lives of superheavy nuclei from a modified generalized liquid-drop model. *Phys. Rev. C* **98**, 024625 (2018). <https://doi.org/10.1103/PhysRevC.98.024625>
34. R. Bonnetti and A. Guglielmetti, In: *Heavy elements and related new phenomena* edited by R. K. Gupta and W. Greiner (World Scientific Pub., Singapore, 1999) vol 2, p. 643
35. R. Bonetti, A. Guglielmetti, Cluster radioactivity: an overview after twenty years. *Rom. Rep. Phys.* **59**, 301 (2007)
36. K.P. Santhosh, T.A. Jose, Cluster pre-formation probabilities and decay half-lives for trans-lead nuclei using modified generalised liquid drop model (MGLDM). *Pramana J. Phys.* **95**, 162 (2021). <https://doi.org/10.1007/s12043-021-02187-w>
37. M. Wang, G. Audi, F.G. Kondev et al., The AME2016 atomic mass evaluation (II). Tables, graphs and references. *Chin. Phys. C* **41**, 030003 (2017). <https://doi.org/10.1088/1674-1137/41/3/030003>
38. H. Koura, T. Tachibana, M. Uno et al., Nuclidic mass formula on a spherical basis with an improved even-odd term. *Prog. Theor. Phys.* **113**, 305 (2005). <https://doi.org/10.1143/PTP.113.305>
39. Y.Z. Wang, S.J. Wang, Y. Hou et al., Systematic study of  $\alpha$ -decay energies and half-lives of superheavy nuclei. *Phys. Rev. C* **92**, 064301 (2015). <https://doi.org/10.1103/PhysRevC.92.064301>
40. D.N. Poenaru, H. Stocker, R.A. Gherghescu, Cluster and alpha decay of superheavy nuclei. *Eur. Phys. J. A* **54**, 14 (2018). <https://doi.org/10.1140/epja/i2018-12469-6>
41. O.N. Ghodsi, M. Morshedloo, M.M. Amiri, Systematic study of heavy-cluster radioactivity from superheavy nuclei. *Phys. Rev. C* **109**, 024612 (2024). <https://doi.org/10.1103/PhysRevC.109.024612>
42. A. Bohr, B.R. Mottelson, *Mat. Fys. Medd.-K. Dan. Vidensk. Selsk.* **30**, 1 (1955)
43. J.M. Allmond, J.L. Wood, Empirical moments of inertia of axially asymmetric nuclei. *Phys. Lett. B* **767**, 226 (2017). <https://doi.org/10.1016/j.physletb.2017.01.072>
44. X.J. Bao, S.Q. Guo, H.F. Zhang et al., Competition between  $\alpha$ -decay and spontaneous fission for superheavy nuclei. *J. Phys. G Nucl. Part Phys.* **42**, 085101 (2015). <https://doi.org/10.1088/0954-3899/42/8/085101>
45. Yu. TsOganessian, A. Sobiczewski, G.M. Ter-Akopian, Superheavy nuclei: from predictions to discovery. *Phys. Scr.* **92**, 023003 (2017). <https://doi.org/10.1088/1402-4896/aa53c1>

Springer Nature or its licensor (e.g. a society or other partner) holds exclusive rights to this article under a publishing agreement with the author(s) or other rightsholder(s); author self-archiving of the accepted manuscript version of this article is solely governed by the terms of such publishing agreement and applicable law.